A
Dissertation
on

Synthesis and Characterisation of Molybdenum Disulphide (MoS_2) Nanopowders

Submitted in partial fulfillment of the requirements for the award of

the degree of

MASTER OF SCIENCE

in

Physics

Submitted by

Navpreet Kaur

(301604028)

Under the Supervision of

Dr. O.P.Pandey

(Senior Professor)

School of Physics & Materials Science

Thapar Institute of Engineering and Technology (TIET), Patiala – 147004

July, 2018

CERTIFICATE

This is to certify that this dissertation entitled **'Synthesis and Characterization of Molybdenum Disulphide (MoS_2) Nanopowders'** is submitted by **Ms. Navpreet Kaur (301604028)** in fulfilment of requirement for the award of degree of Master of Science in Physics from School of Physics and Materials Science, Thapar Institute of Engineering and Technology, Patiala, India. It is an exclusive record of candidate's own research work under the supervision of **Dr. O. P. Pandey**. The dissertation in part or in full has not been submitted in any other university or institute for the award of any degree.

Dr. O. P. Pandey
(Supervisor)
Senior Professor
School of Physics and Materials Science
Thapar Institute of Engineering and Technology, Patiala

DECLARATION

I hereby declare that the work been presented in this thesis report entitled **'Synthesis and Characterization of Molybdenum Disulphide (MoS_2) Nanopowders'** by me in partial fulfilment of the requirements for the award of degree of **Master of Science** in **Physics,** Thapar Institute of Engineering and Technology, Patiala is an authentic award record on my work carried out under the supervision of **Dr. O. P. Pandey** (Senior Professor), School of Physics and Materials Science, Thapar Institute of Engineering and Technology, Patiala. The matter presented in this report has not been submitted in any other university/institute for award of master and science or any other degree.

Navpreet Kaur

Navpreet Kaur

Regd no: 301604028

ACKNOWLEDGEMENT

First and foremost, I would like to express my gratitude and acknowledgement to my M.Sc dissertation thesis supervisor **Dr. O. P. Pandey** (Senior Professor & Head, School of Physics and Materials Science); who has an attitude and substance of a genius; who has continually and convincingly conveyed a spirit of adventure in regard to research. I would also like to thank him for his useful comments, remarks, motivation and constant support provided throughout this course work.

I also express my heartiest gratitude to **Prof. Prakash Gopalan**, Director, Thapar Institute of Engineering and Technology, Patiala, for providing the resources for my research work. I express my sincere thanks to **Dr. Manoj Kumar Sharma** for allowing me to carry out this thesis project.

I proudly grab this opportunity to express my thanks to **Mr. Rameez Ahmad Mir** for guiding and supporting me throughout this research project. Without his guidance and persistent help, this project would not have been possible. I am thankful for his valuable engagement and encouragement. I also express my gratitude to **Dr. Gurbinder Kaur** for her moral support and encouragement. I would like to thank my lab mates who have supported me through thick and thin **Mr. Aayush Gupta**, **Mr. Piyush Sharma**, **Ms. Ruby Priya**, **Ms. Damandeep Kaur, Ms Raveena Khicher, Ms. Neha Singla** and **Ms. Jaspreet Kaur**, who have willingly shared their precious time during this process.

I am highly grateful to my family for standing by my side as a pillar of strength and always pushing me further ahead. I would love to mention my gratitude to my parents **Mr. Dalbir Singh** and **Mrs. Daljit Kaur**, my brother **Mr. Manpreet Singh** and my grandparents; without their blessings I wouldn't have completed this project.

This acknowledgment is incomplete without thanking the people, I was around during this particular period of time, for hearing me out and keeping me harmonious.

And above all I express my indebtness to the almighty for all his blessings.

Navpreet Kaur

Navpreet Kaur

ABSTRACT

Nowadays, sustainably developed society with low carbon content is needed due to vulnerable increase in the global energy demand and to tackle the global warming. The stable and flexible high energy conversion and storage devices such as lithium-ion batteries and super-capacitors have attracted a great attention. In order to enhance the utility of these devices, a highly efficient, stable and cost effective catalytic material is required. In this scenario, the molybdenum disulphide has emerged as a promising catalyst due to its unique properties such as layered structure, high abundance, low cost and advantages over semi-metallic character of graphene. In the present study, the nano-size single phase molybdenum disulphide has been synthesized at 700 °C via single step reduction-sulphurization method in a specially designed autoclave. The structural and morphological properties are investigated by X-ray diffraction (XRD) technique, field emission scanning electron microscopy (FESEM) and high-resolution transmission electron microscopy (HRTEM). The optical properties and band gap of as-prepared nanoparticles are studied by UV-Visible spectroscopy. Both direct and indirect band gap were calculated from reflectance UV-Vis spectroscopy. The reaction mechanism based on these results has been proposed. The as-synthesized samples are expected to be promising catalyst in hydrogen evolution reaction (HER) and their use as electrodes in lithium ion batteries.

List of Figures

Page

Chapter 1

Chapter 3

Chapter 4

List of Tables Page

Chapter 1

Chapter 3

Chapter 4

Table of contents

Chapter 4

30-49

Chapter 5

Chapter 6

1. Introduction

In the past few years, wide range of research interests had been focused on topic of chalcogenides owing to their potential applications in optical, thermal and electrical fields [1-4]. The term chalcogen is formed by Greek words 'chalco' and 'gen' meaning ore formation [5]. The three elements of group VI of modern periodic table *i.e.* sulphur, selenium and tellurium are known as chalcogens. All chalcogens have six electrons in their valence shell. The electronic configuration of these compounds can be stated as ns^2p^4, where the s-orbital of outermost valence shell contains two electrons and p-orbital is occupied by four electrons. The lone pair of s-orbital is generally inert and in p-orbitals two unpaired electrons occupy two p-orbitals and a pair of electrons occupies the third p-orbital [6]. So, they occur in many oxidation states as -2, +2, +4 and +6. A special class of compounds which contain one or more chalcogen atoms as a major constituent connected to another element is known as chalcogenides [6]. The low electronegativity of chalcogens is mainly responsible for covalent bonds formed by them [7]. While bonding, the s and p orbitals of chalcogens most possibly hybridise to form zinc blend structure through sp^3 hybridisation [6]. Out of these chalcogens, sulphur and selenium are non-metals, whereas tellurium is a metalloid [8,9]. When these chalcogens get attached to any transition metal, they give rise to a special class of compounds, called transition metal dichalcogenides (TMDCs) [6]. The general chemical formula for transition metal dichalcogenides is MX_2, where M stands for any transition metal and X represents a chalcogen atom as S (sulphur), Se (selenium) or Te (tellurium)[10,11]. The distinct unison of direct band gap, similarity to graphene layered structure, mono or few layer thickness, absence of dangling bond, supermagnetism phenomenon make TMDCs an appealing focus for research projects [11–13]. Among all the chalcogens, sulphides have a myriad of applications making them the most studied compounds for industrial and research work [14,15]. Sulphides refer to a class of compounds which contain sulphur atom as major anion (S^{-2}) attached to some other positively charged atom, such as zinc sulphide (ZnS), sodium sulphide (Na_2S), nickel sulphide (NiS), hydrogen sulphide (H_2S), copper sulphide (CuS), and molybdenum disulphide (MoS_2). Owing to the existence of multiple oxidation states, small size, low cost, high abundance and clear quantum confinement effects, sulphides occupy important positions in the domain of catalysis, mineralogy, lubrication, photoluminescence and many other fields [16–19].

1.1 Classification of sulphides

Sulphur form many compounds with other positively charged atoms. Depending upon the bonding and electronic structure, the sulphides can be broadly classified into four general categories as shown on Fig.1.1.

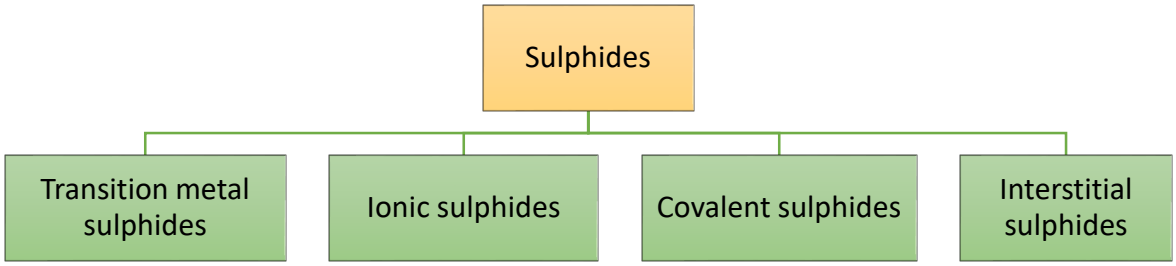

Figure 1.1: General classification of sulphides.

i) **Transition metal sulphides**: The sulphides which form compounds with transition metals with chemical formula MS_2, where M is transition metal and S is sulphide. MoS_2, WS_2, MnS, ZnS, CuS, FeS_2, etc.

ii) **Ionic sulphides**: The compounds containing sulphide attached to the most electropositive element via ionic bonding. Na_2S and Al_2S_3 belong to this category.

iii) **Covalent sulphides**: The covalent sulphides have small electronegative difference between the both species. Certain transition metal sulphides also belong to this category because of their covalent character. The examples are CdS, ZnS and H_2S.

iv) **Interstitial sulphides:** In this category, large electronegativity and atomic size difference exists between metal atom and sulphur. CuS belongs to this category of sulphides.

Depending upon the number of host metal atoms, sulphides can also be categorised as:

- **Binary Sulphides**: The sulphides in which a single metal and one sulphur atom forms the compound. e.g. PbS, Na_2S, FeS_2, H_2S and MoS_2.
- **Ternary sulphides**: Sulphides which contain two different kind of metal atoms attached to a sulphur atom. e.g. Cu_5FeS_4, NiAsS and $CuFeS_2$.
- **Quaternery sulphides**: Three different types of host metal atoms and one sulphur atom results as quaternary sulphides. e.g. $PbCuSbS_3$.

Among all the sulphides, transition metal sulphides are most studied because of their exceptional chemical and physical properties.

1.2 Transition metal disulphides

Metal sulphides have attracted wide range of research interests because of their abundance in nature and unique physical and chemical properties [16]. Transition metals have partially filled d sub-shell or can produce cations having partially filled d sub-shell. When these metals are attached to sulphide, with chemical formula MS_2, they form transition metal sulphides (TMSs) such as MoS_2 (molybdenum disulphide), WS_2 (tungsten disulphide), TiS_2 (titanium sulphide), NiS (nickel sulphide) and CuS (copper sulphide). These compounds have been topic of hot research in solid state physics since the exploitation of graphene [20]. They are widely used for lubrication, catalysis, photoelectric devices and biomedical applications, because of the similarity in layered structures with graphene [10,21,22]. They are known as beyond graphene materials as they overcome the limitations faced in the case of graphene layers [23]. The semi-metallic nature of graphene limits its use in electronics [24,25]. Graphene acts a zero gap material as the conduction and valence band are symmetrical and Fermi surface lies at the point of intersection of these bands [26]. Also, TMDCs are found to be more chemically flexible, in contrast to graphene [11]. For this reason the research interests have been focused from graphene to other layered compounds such as transition metal sulphides [27]. The TMSs are mostly studied because of the unique electronic band structure for band-edge transitions [28,29]. In the past decades, sulphides have attracted a lot of attention throughout the world due to clear quantum confinement effects, when exfoliated to few thick layers [30,31]. TMSs are scientifically and technologically important materials because of their distinct union of direct band gap, atomic layer thickness, strong spin-orbit coupling and lack of inversion symmetry have led to potential applications in areas of photovoltaic devices, lithium ion batteries, hydrogen evolution catalysis, transistors, photodetectors, DNA detection and lubrication [11,30,32–36]. The schematic representation of TMS applications is shown in Fig.1.2.

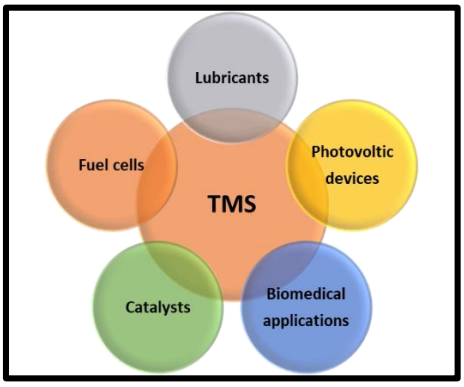

Figure 1.2: Schematic representation of applications of TMS.

In the bulk form, most of the transition metal sulphides have layered structure, which is similar to graphene, with adjacent layers weakly held together because of van der Wall interaction [6,37]. Due to variation in stacking orders and metal atom co-ordination, transition metal sulphides exist in various polytypes [38]. Transition metal sulphides have become subject of much interest because of their ability to form well organised cage structures at nanoscale. These nanomaterials exhibit wide range of unique properties in contrast to their bulk counterparts [34]. The physical properties depend on the number of layers in atomically thin samples of TMSs [6,38]. The electronic structure is such that large band-edge excitation occurs mainly as d-d transitions of metal in contrast to zero bandgap of graphene [26].

1.3 Structure of transition metal disulphides

The total number of transition metal dichalcogenides as observed in nature is about sixty in number. Almost two-thirds of them have layered structure. Only some of these layered compounds exist naturally, others are synthesised compounds [6].

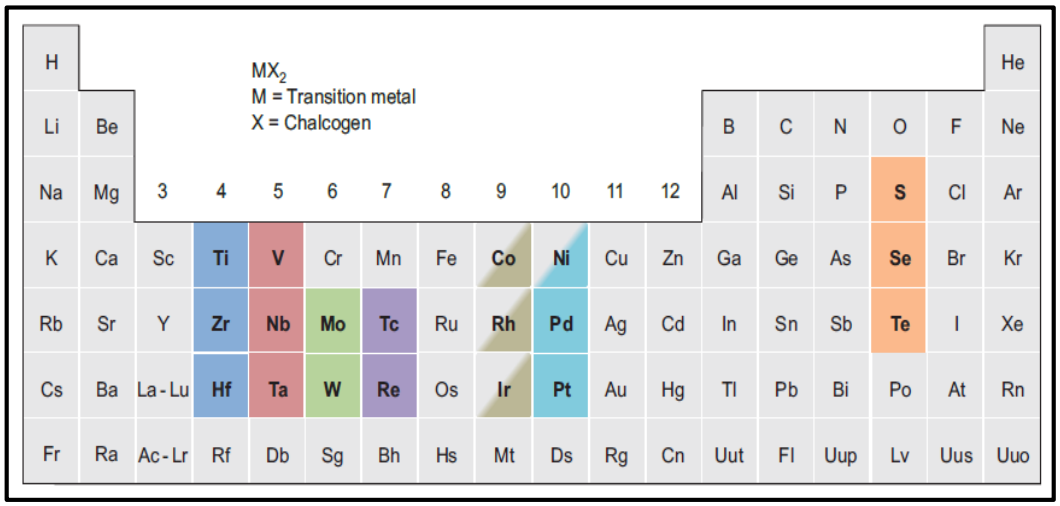

Figure 1.3: TMDCs having layered structure have been marked on periodic table, showing three chalcogen atoms in orange colour [11].

The structure of transition metal sulphides consist of layers in which in-plane atoms are covalently connected, whereas the layers themselves have weak van der Waals forces [39]. Three atomic planes, each 6-7Å thick, are contained in each layer [6,11]. The planes are hexagonally packed and the hexagonal plane of metal atoms is sandwiched between chalcogen (sulphur) atoms as shown in Fig.1.4 (a). In these compounds, high oxidation states of transition metals are not observed, because of small electronegativity of chalcogens [7]. During the

bonding of transition metals and sulphur the d-orbitals electrons of sulphur participate, strengthening the bonds and favouring the trigonal-prismatic coordination in sulphur as shown in Fig.1.4 (b). The distortions in the structures are due to large polarizability of sulphur ions arisen due to d-orbital participation [6,34].

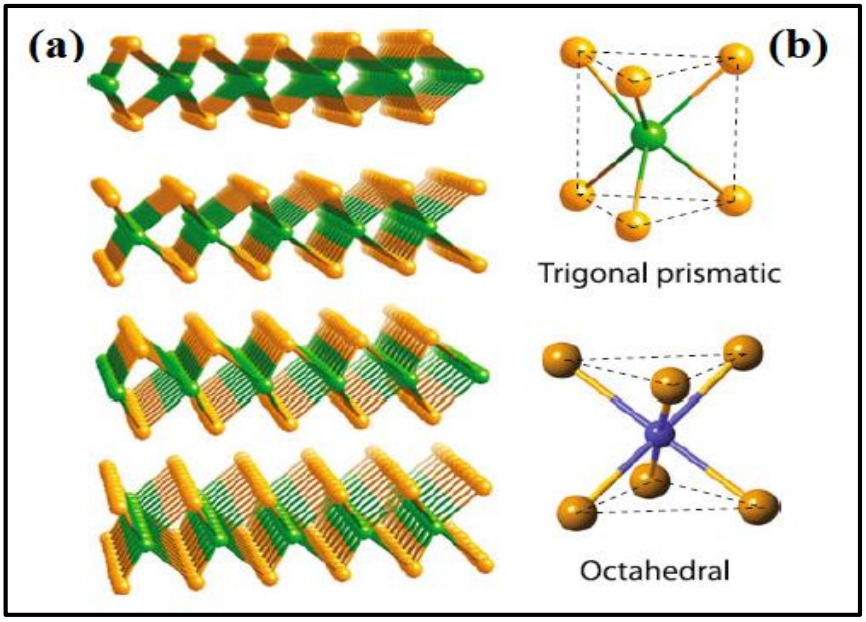

Figure 1.4: (a) 3-D representation of typical MX_2 structure, where metal atoms are shown in green and chalcogen in orange, (b) Transition metals can have trigonal prismatic or octahedral coordination. [34]

The occurrence of polymorphs of a same TMSs is also common. For example, natural molybdenum disulphide (MoS_2) usually exists as 2H phase, while the one synthetically fabricated has 3R phase. The metal coordination in both these polymorphs is trigonal prismatic implying that stacking sequence has no impact on metal coordination [6].

1.4 Properties of transition metal disulphides

The transition metal disulphides exhibit different physical and chemical properties depending upon their structural, morphological aspects as given below:

- The phenomenon of superconductivity is observed in all TMSs, resulting in a new class of artificial 2-D superconductors. The superconductivity is directly related to asymmetric spin-orbit coupling (ASOC) [40].
- TMS monolayers exhibit direct band gap because of d-d transitions occurring in metal atom. They have been most popularly used in transistors nowadays as it had made

possible to switch on-off the circuit, owing to this direct band-gap. TMS monolayer band gaps lie in visible range (400-700 nm) [40,41].

- No inversion centre has been detected in TMDC monolayers. As a result, the occurrence of valleytronics is observed in them, which allows a new degree of freedom to charge carriers in these 2-D materials. This also leads to piezoelectricity in odd layers of these materials [40,42].
- They possess higher carrier mobility and high on/off ratio [29].
- The Young's modulus of TMSs is reported to be higher than even of steel. Layers of TMSs can bear deformation upto a certain percentage before fracturing [26,43].

2. Molybdenum disulphide

Among different TMSs, molybdenum disulphide (MoS_2) having layered structure resembling to structure of graphene is mostly studied because of exceptional chemical properties. This unique layered structure endows MoS_2 many novel properties, such as chemical stability, anisotropy and anti-photo corrosion [37]. Owing to its distinctive catalytic, electronic and optical properties, it is widely used in numerous areas, such as hydrosulfurization catalyst, photo and electrocatalyst, in lithium batteries and as dry lubricant [18,35,44]. The enhancement of surface properties of nano MoS_2 makes it promising candidate for water splitting by both photo and electro catalysis for hydrogen production as clean and renewable energy source [45-47]. The catalysis and efficiency of hydrogen evolution reaction (HER) is greatly influenced by surface characteristics and method of synthesis [36]. The synthesis of MoS_2 at nano scale with uniform sulphurization and controlled morphology is highly desirable.

Molybdenum disulphide mainly occurs as mineral Molybdenite (chief ore of molybdenum) in nature [48]. Molybdenum disulphide is an inorganic compound made of Molybdenum and Sulphur, with chemical formula MoS_2, where molybdenum belongs to transition metals and sulphur is a chalcogen. Molybdenum exists in various oxidation states as +2, +4 and +6 and oxidation state of sulphide is -2, thus forming various compounds as MoS_3, MoS_3 and Mo_2S_3. MoS_2 having oxidation state of Mo (+4) forms the stable and prominent member of transition metal sulphide family. MoS_2 layers are assembled together by weak van der Wall interactions, so that they can easily move against each other and is used for dry lubricant applications [49]. MoS_2 has a very high melting point above 1,185^{o}C. Bulk MoS_2 is an indirect bandgap semiconductor with bandgap of 1.23 eV, whereas the monolayer of MoS_2 has direct bandgap of 1.8eV [41]. Typically, the Mo-S bond is 2.42 Å long and a single layer of MoS_2 is 0.7 nm

thick. It is a promising agent for novel diverse applications in areas of electronics, optoelectronics, sensors and energy-storage devices [28]. The similarity of MoS_2 with graphene and bandgap variation widens its industrial use as catalyst for hydrogen production and storage applications [36]. MoS_2 having the unique property of band gap variation is a promising low cost efficient catalyst and support for HER via photocatlysis and electrolcatlysis [50].

2.1 Structure of molybdenum disulphide

MoS_2 is a naturally occurring layered solid with structure similar to graphene layers [37]. The crystal structure of MoS_2 consists of weakly coupled layers of S-Mo-S with Mo atom layer sandwiched in between two S atom layers. The unit cell of MoS_2 has covalently bonded S-Mo-S in a hexagonal arrangement, where each S atom coordinates with three Mo atoms in the form of trigonal prismatic coordination [50]. MoS_2 has three main types of phases described as: 1T, 2H and 3R MoS_2 as shown below in Fig.1.5 (a-c), respectively. The coordination of molybdenum atoms in 1T Fig.1.5 (a) form is distorted octahedral, whereas 2H and 3R Fig.1.5 (b,c) crystalline varieties differ by layer arrangement. The metastable 1T phase can transform to 2H phase by heating treatment [11].

Poly-Types of MoS_2

The metastable 1T phase as shown below in Fig.1.5 (a) is metallic modification of monolayered molybdenum disulphide. It contains one layer (S-Mo-S) per unit cell stack in tetragonal symmetry with octahedral coordination. Monolayer of 1T MoS_2 consists of two slabs of hexagonally packed S atoms with one slab of hexagonal Mo atoms sandwiched in between them. Mo atoms occupy centre positions of octahedral interstices of the S layers. Here, the S atoms in upper and lower planes are offset from each other. The metallic phase possesses unique electrical properties [29,37,50].

Bulk MoS_2 exists as 2H phase and contains two layers per unit cell stack in hexagonal symmetry with trigonal prismatic coordination as shown in Fig.1.5 (b). This is a stable phase and dominates in nature. Each Mo atom in this phase is surrounded by six S atoms, as in a trigonal prism with stacking sequence of AbA BaB. There is strong chemical bonding between the atoms but layers have weak van der Waals force between them [37,40,50].

3R MoS_2 consists of three layers per unit cell stack in the rhombohedral symmetry with trigonal prismatic coordination in 3R phase as shown in Fig.1.5 (c). The stacking sequence of planes is AbA CaC BcB. This poly-type exists at high pressure i.e. above 4.0 GPa [6,37,50].

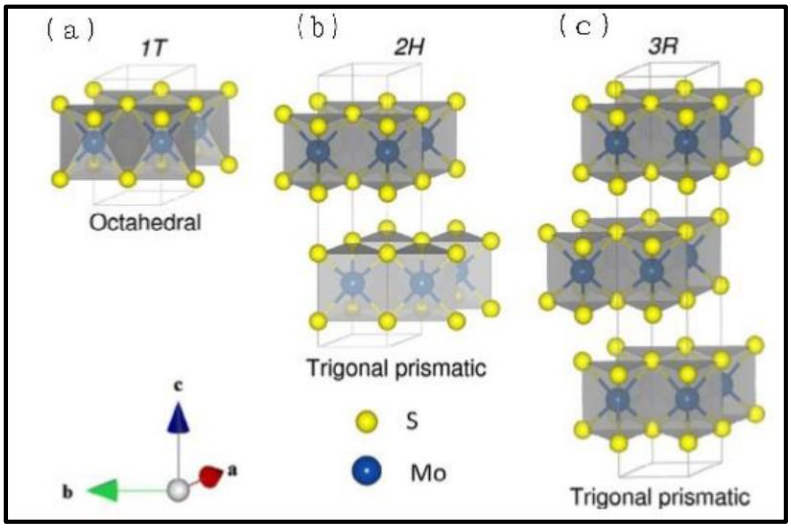

Figure 1.5: Polytypes of MoS_2 (a) 1T: tetragonal symmetry, (b) 2H: hexagonal symmetry, (c) 3R: rhombohedral symmetry. [50]

2.2 Properties of molybdenum disulphide

MoS_2, a black shiny powder has molar mass of 160.07 g/mol with density 5.06 g/cm^3. It melts at temperature only higher than 1000 °C. Young's Modulus for MoS_2 is reported to be 0.33±0.07 TPa, making it a mechanically flexible material [26]. MoS_2 is found to be diamagnetic in nature [11]. In addition, MoS_2 is found quite stable against photocorrosion, making it a potential candidate for photo and electrochemical applications [37].

The physical properties of molybdenum disulphide are given in Table 1.1.

Table 1.1: Properties of molybdenum disulphide.

Parameters	Polytypes	
	2H	3R
Lattice parameters (a,c)	a = 3.16 Ă	a = 3.17 Ă
	c = 12.29 Ă	c = 18.38 Ă
Resitivity (ρ)	33 Ωcm	0.3 Ωcm
Electron concentration (n)	$6 \cdot 10^{15}$ cm^{-3}	
Energy gap (E_g)	1.971 eV (at T=77K)	1.9 eV
Hall coefficient (μ_H)	57 cm^2/V s	

Most of chemical properties depends directly on number and sequence of stacking pattern of layers. It also shows some interesting optical properties, as in photoluminescence spectra, two

distinct peaks (A1 and B1 excitons) are observed at 670nm and 627nm, but with increase in number of layers they disappear [26]. Also, the transition of band gap into a direct one has led to higher mobility and increased current on/off ratio in MoS_2 [41]. This band gap transition has led to physical phenomenon of valleytronics. Owing to this phenomenon and lack of inversion symmetry, the odd number layers in MoS_2 are piezoelectric [11]. While reacting chemically, the metallic edge planes with existence of sulphur vacancies appear as active sites, whereas, the sulphur atoms lying on basal planes behave as inert as they are completely coordinated. Moreover, the poisonous behaviour of sulphur is no longer observed in MoS_2. The metallic states located at edges act as catalytic sites as they can accept or donate electrons. All these points result in high activity of molybdenum disulphide [37].

2.3 Applications of molybdenum disulphide

i) **Photo and Electrocatalysis**: The importance of MoS_2 as a catalyst is because of of its relatively high activity and resistance to poisoning with sulphur. It is widely used in hydro-desulfurization and hydrogen evolution reactions (HER). It is also used in hydrogenation of CO and methanation [37].

ii) **Batteries**: MoS_2 has been verified as efficient electrode material for lithium ion batteries (LIBs). LIBs have high operating voltage, large energy density and long life cycle. They consist of anode, cathode and electrolyte. MoS_2 has proved to a good anode as well as cathode candidate in LIBs, making it widely usable in field of energy conversion and storage [44].

iii) **Bio-applications**: MoS_2 has good biocompatibility, therefore is used for DNA optical detection, artificial protein receptors, and glucose electrochemical sensing, efficient photothermal therapy, enzymatic biodegradation, combined therapy and multifunctional cancer theranostic. MoS_2 is the only known biodegradable material that can be ultimately excreted from body [51].

iv) **Sensors**: MoS_2 has been used to develop various types of sensors, such as optical sensors, gas sensors, chemical sensors, and biosensors, owing to their high surface-to area ratio as well as their unique physical and chemical properties [28].

v) **Lubricant**: Molybdenum disulphide nanoparticles are known to possess tribological properties. Because of MoS_2 lamellar structure with weak van der wall forces between layers, it works as an excellent solid lubricant [37].

2.4 Synthesis of MoS_2

Different physical and chemical methods have been applied to synthesise nano-sized molybdenum disulphide bulk and nanostructures. The physical methods involve high energy techniques such as microwave plasma, sputtering or pulsed-laser deposition. All these methods are rapid and obtained nanostructures result in reduced surface areas [37]. Chemical route include multi-step methods as high temperature transport, hydrothermal, solvothermal and sonochemical synthesis [25]. Chemical synthesis methods have proved to be facile; cost efficient and resultant particles are highly pure with controlled morphologies [52]. Till date, only limited reports are available on morphology controlled techniques [53]. The reported synthesis methods mostly occur over a long duration of time with involvement of multi-steps, costing financial resources and energy exploitation. So, a single step method is the need of the hour through which we can synthesize molybdenum disulphide nanoparticles in a limited amount of time. The further knowledge on the behaviour of molybdenum and sulphur phase formation can be gathered from the detailed study of phase diagram of MoS_2 as given in Fig.1.6.

2.4.1 Phase diagram of MoS_2

The Fig.1.6 shows the phase diagram of Mo-S system. The two stable phases according to the phase diagram are Mo_2S_3 (belonging to group *m*P10) and MoS_2 (from group *h*P6). A metastable phase of MoS_2 (*h*R3) also exists, which has a close structure to *h*P6.

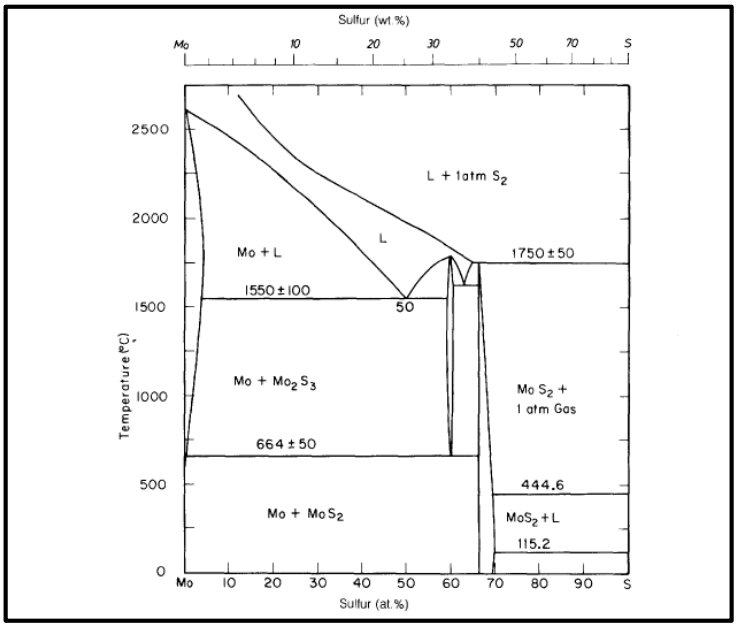

Figure 1.6: Phase diagram of MoS_2. [54]

It has been reported that the content of molybdenum is higher in *h*R3 than *h*P6. The *h*R3 state is found stable at higher pressures. When the amount of sulphide increases in *h*P6 phase, expansion and distortion occurs in the lattice upto $MoS_{2.59}$. There are more chances of obtaining an amorphous phase, with increase in sulphur content. The equilibrium phase of MoS_2 changes to $MoS_{2.2}$ if the temperature is increased upto 1100 °C [54]. According to the thermodynamic values, *h*P6 symmetry of MoS_2 is most stable with -1.19±0.01 value of entropy ($\Delta H°_{298}/R$), K and free energy function ($\Delta G°_{298}/R$), K value of -10720±100.

References

[1] J. Sanghera and I. Aggarwal, "Active and passive chalcogenide glass optical fibers for IR applications: a review," *J. Non. Cryst. Solids*, vol. 256–257, pp. 6–16, 1999.

[2] B. J. Eggleton, B. Luther-Davies and K. Richardson, "Chalcogenide photonics," *Nat. Photonics*, vol. 5, no. 3, pp. 141–148, 2011.

[3] M. Stafe *et al.*, "Numerical simulations of surface plasmon resonances in metal-chalcogenide waveguides," *Proc. SPIE - Int. Soc. Opt. Eng.*, vol. 9258, pp. 1–7, 2015.

[4] D. S. Wang, W. Zheng, C. H. Hao, Q. Peng and Y. D. Li, "A synthetic method for transition-metal chalcogenide nanocrystals," *Chem. - A Eur. J.*, vol. 15, no. 8, pp. 1870–1875, 2009.

[5] A. Quayoum, "Review on Chalcogenide glass," vol. 2, no. 2, pp. 147–154, 2017.

[6] A. V. Kolobov and J. Tominaga, *Two-Dimensional Transition-Metal Dichalcogenides*, vol. 239. 2016.

[7] F. Jellinek, "Transition Metal Chalcogenides. Relationthip between chemical composition, crystal structure and physical properties," *React. Solids*, vol. 5, pp. 323–339, 1988.

[8] C. C. Reddy and E. J. Massaro, "Biochemistry of selenium: A brief overview," *Toxicol. Sci.*, vol. 3, no. 5, pp. 431–436, 1983.

[9] S. Wang, "Tellurium, its resourcefulness and recovery," *Jom*, vol. 63, no. 8, pp. 90–93, 2011.

[10] K. Shomalian, M. M. Bagheri-Mohagheghi and M. Ardyanian, "Synthesis and characterization of porous nanoparticles of molybdenum sulfide (MoS_2) chalcogenide semiconductor prepared by polymerizing-complexing sol–gel method," *J. Mater. Sci. Mater. Electron.*, vol. 28, no. 19, pp. 14331–14340, 2017.

[11] M. Chhowalla, H. S. Shin, G. Eda, L. J. Li, K. P. Loh and H. Zhang, "The chemistry of two-dimensional layered transition metal dichalcogenide nanosheets," *Nat. Chem.*, vol. 5, no. 4, pp. 263–275, 2013.

[12] R. Ganatra and Q. Zhang, "Few-Layer MoS_2 : A Promising Layered Semiconductor," *ACS Nano*, vol. 8, no. 5, pp. 4074–4099, 2014.

[13] H. Yuan, L. Kong, T. Li and Q. Zhang, "A review of transition metal chalcogenide/graphene nanocomposites for energy storage and conversion," *Chinese Chem. Lett.*, vol. 28, no. 12, pp. 2180–2194, 2017.

[14] S. J. Pickart, "Physical Properties of Sulfide Materials," *Mineral. Soc. Am. Spec. Pap.*, vol. 3, pp. 145–153, 1970.

[15] M. Rajamathi and R. Seshadri, "Oxide and chalcogenide nanoparticles from hydrothermal/solvothermal reactions," *Curr. Opin. Solid State Mater. Sci.*, vol. 6, no. 4, pp. 337–345, 2002.

[16] S. Wang, C. An and J. Yuan, "Synthetic fabrication of nanoscale MoS_2-based transition metal sulfides," *Materials (Basel).*, vol. 3, no. 1, pp. 401–433, 2010.

[17] H. S. Genin and J. A. Ibers, *Transition Metal Sulphides*, vol. 60. 1998.

[18] R. R. Chianelli *et al.*, "Catalytic Properties of Single Layers of Transition Metal Sulfide Catalytic Materials," *Catal. Rev.*, vol. 48, no. 1, pp. 1–41, 2006.

[19] W. Tang *et al.*, "In Situ Observation and Electrochemical Study of Encapsulated Sulfur Nanoparticles by MoS_2 Flakes," *J. Am. Chem. Soc.*, vol. 139, no. 29, pp. 10133–10141, 2017.

[20] C. N. R. Rao, U. Maitra and U. V. Waghmare, "Extraordinary attributes of 2-dimensional MoS_2 nanosheets," *Chem. Phys. Lett.*, vol. 609, pp. 172–183, 2014.

[21] Q. Liu *et al.*, "Gram-Scale Aqueous Synthesis of Stable Few-Layered 1T-MoS_2: Applications for Visible-Light-Driven Photocatalytic Hydrogen Evolution," *Small*, vol. 11, no. 41, pp. 5556–5564, 2015.

[22] X. Xu, W. Liu, Y. Kim and J. Cho, "Nanostructured transition metal sulfides for lithium ion batteries: Progress and challenges," *Nano Today*, vol. 9, no. 5, pp. 604–630, 2014.

[23] S. A. Han, R. Bhatia and S.-W. Kim, "Synthesis, properties and potential applications of two-dimensional transition metal dichalcogenides," *Nano Converg.*, vol. 2, no. 1, p. 17, 2015.

[24] J.-F. C. G Deokar, D Vignaud, R Arenal and P Louette, "Synthesis and characterization of vertically standing MoS_2 nanosheets," *Sci. Rep.*, vol. 21171, no. 6, pp. 1–9, 2016.

[25] A. Gupta, T. Sakthivel and S. Seal, "Recent development in 2D materials beyond graphene," *Prog. Mater. Sci.*, vol. 73, pp. 44–126, 2015.

[26] X. Li and H. Zhu, "Two-dimensional MoS_2: Properties, preparation, and applications," *J. Mater.*, vol. 1, no. 1, pp. 33–44, 2015.

[27] N. A. Kumar, M. A. Dar, R. Gul and J. B. Baek, "Graphene and molybdenum disulfide hybrids: Synthesis and applications," *Mater. Today*, vol. 18, no. 5, pp. 286–298, 2015.

[28] X. Zhang, Z. Lai, C. Tan and H. Zhang, "Solution-Processed Two-Dimensional MoS_2 Nanosheets: Preparation, Hybridization, and Applications," *Angew. Chemie - Int. Ed.*,

vol. 55, no. 31, pp. 8816–8838, 2016.

[29] Q. H. Wang, K. Kalantar-Zadeh, A. Kis, J. N. Coleman and M. S. Strano, "Electronics and optoelectronics of two-dimensional transition metal dichalcogenides," *Nat. Nanotechnol.*, vol. 7, no. 11, pp. 699–712, 2012.

[30] A. Kuc, N. Zibouche and T. Heine, "Influence of quantum confinement on the electronic structure of the transition metal sulfide TS_2," *Phys. Rev. B - Condens. Matter Mater. Phys.*, vol. 83, no. 24, pp. 1–4, 2011.

[31] M. Chhowalla, Z. Liu and H. Zhang, "Two-dimensional transition metal dichalcogenide (TMD) nanosheets," *Chem. Soc. Rev.*, vol. 44, no. 9, pp. 2584–2586, 2015.

[32] C. N. R. Rao and K. P. R. Phisharody, "Transition metal sulfides," *Prog. Solid State Chem.*, vol. 10, pp. 207–270, 1974.

[33] L. Hu, Y. Ren, H. Yang and Q. Xu, "Fabrication of 3D Hierarchical MoS_2 /Polyaniline and MoS_2 /C Architectures for Lithium-Ion Battery Applications," *ACS Appl. Mater. Interfaces*, vol. 6, no. 16, pp. 14644–14652, 2014.

[34] R. Lv *et al.*, "Transition metal dichalcogenides and beyond: Synthesis, properties, and applications of single- and few-layer nanosheets," *Acc. Chem. Res.*, vol. 48, no. 1, pp. 56–64, 2015.

[35] Y. Li, H. Wang, L. Xie, Y. Liang, G. Hong and H. Dai, "MoS_2 nanoparticles grown on graphene: An advanced catalyst for the hydrogen evolution reaction," *J. Am. Chem. Soc.*, vol. 133, no. 19, pp. 7296–7299, 2011.

[36] A. B. Laursen, S. Kegnæs, S. Dahl and I. Chorkendorff, "Molybdenum sulfides—efficient and viable materials for electro- and photoelectrocatalytic hydrogen evolution," *Energy Environ. Sci.*, vol. 5, no. 2, p. 5577, 2012.

[37] Z. He and W. Que, "Molybdenum disulfide nanomaterials: Structures, properties, synthesis and recent progress on hydrogen evolution reaction," *Appl. Mater. Today*, vol. 3, pp. 23–56, 2016.

[38] D. Jariwala, V. K. Sangwan, L. J. Lauhon, T. J. Marks, and M. C. Hersam, "Emerging Device Applications for Semiconducting Two-Dimensional Transition Metal Dichalcogenides Deep," *ACS Nano*, vol. 8, no. 2, pp. 1102–1120, 2014.

[39] J. A. Wilson and A. D. Yoffe, "The transition metal dichalcogenides discussion and interpretation of the observed optical, electrical and structural properties," *Adv. Phys.*, vol. 18, no. 73, pp. 193–335, 1969.

[40] S. Manzeli, D. Ovchinnikov, D. Pasquier, O. V. Yazyev and A. Kis, "2D transition metal dichalcogenides," *Nat. Rev. Mater.*, vol. 2, 2017.

[41] B. Radisavljevic, A. Radenovic, J. Brivio, V. Giacometti and A. Kis, "Single-layer MoS_2 transistors," *Nat. Nanotechnol.*, vol. 6, no. 3, pp. 147–150, 2011.

[42] R. Suzuki *et al.*, "Valley-dependent spin polarization in bulk MoS_2 with broken inversion symmetry," *Nat. Nanotechnol.*, vol. 9, no. 8, pp. 611–617, 2014.

[43] D. Akinwande *et al.*, "A Review on Mechanics and Mechanical Properties of 2D Materials - Graphene and Beyond," *Extrem. Mech. Lett.*, vol. 13, pp. 42–77, 2016.

[44] Y. Zhao, Y. Zhang, Z. Yang, Y. Yan and K. Sun, "Synthesis of MoS_2 and MoO_2 for their applications in H_2 generation and lithium ion batteries: A review," *Sci. Technol. Adv. Mater.*, vol. 14, no. 4, 2013.

[45] X. L. Yin *et al.*, "MoS_2/CdS Nanosheets-on-Nanorod Heterostructure for Highly Efficient Photocatalytic H_2 Generation under Visible Light Irradiation," *ACS Appl. Mater. Interfaces*, vol. 8, no. 24, pp. 15258–15266, 2016.

[46] J. Sun, L. Duan, Q. Wu and W. Yao, "Synthesis of MoS_2 quantum dots cocatalysts and their efficient photocatalytic performance for hydrogen evolution," *Chem. Eng. J.*, vol. 332, pp. 449–455, 2018.

[47] B. Sun, F. Shan, X. Jiang, J. Ji and F. Wang, "One-pot synthesis of MoS_2/In_2S_3 ultrathin nanoflakes with mesh−shaped structure on indium tin oxide as photocathode for enhanced photo-and electrochemical hydrogen evolution reaction," *Appl. Surf. Sci.*, vol. 435, pp. 822–831, 2018.

[48] E. Benavente, M. A. Santa Ana, F. Mendizábal and G. González, "Intercalation chemistry of molybdenum disulfide," *Coord. Chem. Rev.*, vol. 224, no. 1–2, pp. 87–109, 2002.

[49] C. Lee, H. Yan, L. Brus, T. Heinz, J. Hone and S. Ryu, "Anomalous lattice vibrations of single-and few-layer MoS_2," *ACS Nano*, vol. 4, no. 5, pp. 2695–700, 2010.

[50] B. Han and Y. H. Hu, "MoS_2 as a co-catalyst for photocatalytic hydrogen production from water," *Energy Sci. Eng.*, vol. 4, no. 5, pp. 285–304, 2016.

[51] L. Chen *et al.*, "One-Pot Synthesis of MoS_2 Nanoflakes with Desirable Degradability for Photothermal Cancer Therapy," *ACS Appl. Mater. Interfaces*, vol. 9, no. 20, pp. 17347–17358, 2017.

[52] S. X. Hou, C. Wu and Y. J. Huo, "Controllable preparation of nano molybdenum disulfide by hydrothermal method," *Ceram. - Silikaty*, vol. 61, no. 2, pp. 158–162, 2017.

[53] S. V. P. Vattikuti, C. Byon, C. V. Reddy, J. Shim and B. Venkatesh, "Co-precipitation synthesis and characterization of faceted MoS_2 nanorods with controllable morphologies," *Appl. Phys. A Mater. Sci. Process.*, vol. 119, no. 3, pp. 813–823, 2015.

[54] L. Brewer and R. H. Lamoreaux, "The Mo-S system (Molybdenum-Sulfur)," *Bull. Alloy Phase Diagrams*, vol. 1, no. 2, pp. 93–95, 1980.

2. Literature review

Molybdenum disulphide at present is most intensively studied compound in material science on account of its intriguing applications in flexible electronics, biomedical, energy storage and harvesting and electrochemical catalysis. It is also known as beyond graphene compound because of many novel physical, chemical, electronic and catalytic properties when peeled off to atomic-layer thickness. The high activity shown by MoS_2 has appealed the research community to shift focus on large scale applications of molybdenum disulphide in hydrogen production by water splitting. But all these properties depend on the morphology, structure and surface characteristics of synthesised nanoparticles, which depend on method of synthesis. The change in structure, surface composition and phase are observed by varying synthesis parameters. Researchers have focused on developing a feasible, low cost method to synthesize nano-MoS_2 with enhanced catalytic activity. Traditional methods such as mechanical cleavage or exfoliation have gone into oblivion because it is difficult to control size and thickness of resultant samples. In comparison, chemical vapour deposition technique is an efficient method but at the same time it is very costly and requires high-scale machinery. The low cost hydrothermal method requires bulk quantities of precursors along with tedious time duration. So, all these methods have been studied and the recent trends for the synthesis have been reviewed below.

Hu and Hu [1] in 2009 synthesized different MoS_2 nanostructures by heating MoS_3 precursor via precipitation method. The synthesized MoS_3 precursors were then calcined under H_2 gas at high temperatures in the range of 700 to 1000 °C. The as obtained samples were characterized by X-ray diffractometer (XRD), scanning electron microscope (SEM) and transmission electron microscope (TEM). The exfoliation restacking behaviour was also investigated. MoS_2 hollow nanoballs were obtained when thioacetamide (C_2H_5NS) was used as sulphur source, whereas cloud-like loose nanostructures were obtained when Na_2S (sodium sulphide) was used as sulphur source. After exfoliation treatment, it was observed from XRD patterns that restacking was not regular along c axis.

Lin *et al.* [2] in 2010 synthesized MoS_2 nanorods via hydrothermal method. Here, sillicontungstic acid was used as an additive. The structure and morphology of as-obtained samples were characterized by XRD and field emission scanning electron microscope (FESEM). Both hexagonal and rhombohedral phases were observed in the obtained nanorods.

The atomic ratio of Mo:S was found to be 1:2 via XPS data. The FESEM micrographs indicated that MoS_2 nanorods have uniform size with diameter in range of 20-50 nm and 400-500 nm in length. According to the proposed mechanism, MoS_2 layers swelled in presence of sillicontungstic acid leading to the intercalation of small molecules. The swollen compund exfoliated when put into hydrothermal reaction for duration of 24 hours, synthesizing MoS_2 nanorods.

Dong *et al.* [3] in 2011 synthesized MoS_2 nanoflowers via hydrothermal method. The precursors were magnetically stirred after adding ionic liquid for 12 hours and then put into autoclave for 24 hours. The X-ray diffraction patterns indicated pure and highly crystallite structure, confirmed by SAED results. The uniform rose-like morphology with size of 1μm was confirmed by SEM micrographs. TEM and HRTEM images revealed rough surfaces and bent layers of MoS_2. The as prepared nanoflowers had higher specific surface area and more active sites, as the morphology was highly influenced by ionic liquid.

Chen *et al.* [4] in 2012 synthesized MoS_2/CdS photocatalyst via ball milling combined calcination method. These samples were characterised by XRD, TEM and SEM to confirm the size, structure and morphology of as-obtained samples. The smooth-surfaced particles were mostly smaller than 100 nm in size. The TGA/DSC results were found in good agreement to those of XRD patterns. XPS studies and HRTEM images showed that layered MoS_2 was deposited on surface of CdS. The as prepared samples showed enhanced photocatalytic H_2 evolution activity.

Wang *et al.* [5] in 2013 synthesized hollow nanoparticles of molybdenum disulphide by solvothermal method. The above prepared samples were characterized by X-ray diffraction (XRD), transmission electron microscope (TEM), High resolution-TEM (HRTEM) and scanning electron microscope (SEM). The as-prepared MoS_2 consist of spherical nanoparticles with diameter of 300-800 nm with high wrinkled surface. The lattice constant values as calculated from XRD data showed increase in c value in comparison to standard data. These hollow nanoparticles showed improved lithium storage performance than the solid counterparts.

Zhao *et al.* [6] in 2014 synthesized thin MoS_2 nanoflakes encapsulated in carbon nanofibres by hydrothermal method and second method of electro-spinning followed by carbonization. X-ray powder diffractometer (XRD), scanning and transmission electron microscopy revealed MoS_2 nanoflakes suffered expansion in interlayer spacing, resulting in thickness of about 5 nm. SAED patterns were in good reference to that of XRD peaks. Hybrid nanofibrous mats formed by the later method exhibited excellent performance as anode material for LIBs.

Wang *et al.* [7] in 2014 synthesized morphology controlled MoS_2 nanostructures (nanospheres, nanoribbons and aggregated nanoparticles) via introducing variations in surfactants and reaction temperatures of hydrothermal method using different precursors. XRD results referred to 2-H hexagonal phase. The nanoribbons exhibited a smaller crystallite size whereas in aggregated nanoparticles the d-spacing was found to be larger. FESEM and HRTEM images indicated uniform size of rough-surfaced nanostructures close to 600 nm. SAED patterns revealed weak crystallite nature of samples. The results revealed that the final morphology of nanostructure highly depends on surfactant and reaction temperature. The electrochemical measurements revealed that nanospheres possessed highest cycle stability and rate capacity among the synthesized samples, owing to its large specific surface.

Vattikuti *et al.* [8] in 2015 synthesized MoS_2 nanorods via co-precipitation method. The precursors Mo:citric acid were taken in ratio of 1:5, in a pH controlled environment. The transition of nanospheres into nanorods was observed when calcined at 800 °C. XRD, SEM and TEM characterizations revealed that finally nanorods with diameter 200-150 nm and few tens of micrometers long were obtained. UV-Vis spectroscopy revealed that bandgap of such nanorods was less than that of nanospherical structures. The purity of sample was confirmed by EDX mapping. FTIR and TGA curves indicated vapourisation of organic components and recrystallization of MoS_2. The shape and size of nanoparticles was successfully controlled by effect of temperature.

Vattikuti *et al.* [9] in 2015 synthesized MoS_2 multi-wall nanotubes using wet chemical method with H_2O_2 solvent as growth promoter. The size and morphology of as-prepared nanoparticles were characterized by X-Ray diffraction, transmission electron microscopy (TEM) and HRTEM. An increase in the size of nanotubes was observed as per the increase in reaction time. The mean length of as obtained nanotubes was 100-300 nm with diameter 20-30 nm and

energy bandgap was 2.57eV. The sample with 0.5wt% showed greater photocatalytic degradation of dye Rhodamine B (RhB) under UV light irradiation.

Cheah *et al.* [10] in 2015 synthesized 2-H MoS_2 nanospheres via hydrothermal method. The X-ray patterns confirmed hexagonal phase with low crystallinity. The atomic packing was not in systemized order, due to the possibility of strain within internal structure. The morphology by TEM and HRTEM micrographs revealed spherical structure with average diameter of 120-180 nm. Optical absorption spectra showed visible light region occurring electronic transitions.

Yin *et al.* [11] in 2016 synthesized MoS_2/CdS nanosheets-on-nanorod heterostructure via two-step prolonged solvothermal method. TEM and HRTEM images showed discontinuous amorphous lattice fringes on nanosheets. EDS analysis indicated S and Cd were homogenously distributed whereas Mo matched weakly with sheet-like structures. The presence of Cd, Mo, S and O was confirmed by XPS spectrum. XRD data indicated MoS_2 was partially crystallite in nature and its loading was deficient on surface of CdS nanorods. The loading dependent experiments showed that CdS nanosheets-on-nanorods with MoS_2 loading exhibited the highest H_2 generation rate during photocatalytic HER under visible light.

Deokar *et al.* [12] in 2016 synthesized MoS_2 nanosheets with high purity by additive-free chemical vapor deposition (CVD) method. Vertically aligned 2H-MoS_2 nanosheets with large surface area were processed. Raman and TEM analysis indicated 2-H MoS_2 crystal structure in prepared nanosheets. High purity of sample was confirmed by XPS. Thin nanosheets show PL at 1.83eV as that of direct band gap monolayer. Further, photoluminescence showed sharp increase with reduction in thickness.

Yan *et al.* [13] in 2016 synthesized ZnO coated MoS_2 nanosheets by two step hydrothermal method. The structure and morphology of as obtained samples was characterised by XRD, EDS, XPS, FESEM and TEM. The results revealed the flower-like morphology of MoS_2 in a range of 400 to 800 nm diameter. It consisted of many nanosheets with average diameter of 500 nm and about 5-10 nm thick. These ZnO coated MoS_2 nanosheets proved to be better gas sensors towards ethanol than ZnO nanoparticales.

Kumar *et al.* [14] in 2016 synthesized MoS_2 nanostructures in a time span of 10 minutes through supercritical ethanol route method. The as-obtained samples were characterized by XRD, XPS, FESEM, HRTEM, BET and FT-IR spectroscopy. The XRD patterns confirmed hexagonal pure phase of MoS_2. Decrease in interplaner spacing was observed with increase in calcination temperature. The FESEM revealed aggregation of nanoplates, whereas nanoplates merged to form a sheet like structure with increase in calcination temperature. The fringes-distance between well stacked layers was about 0.65 nm as per HRTEM micrographs. The FT-IR spectroscopy indicated presence of hydroxyl groups on surface of MoS_2 nanoparticles. The pore size of the samples was found to be in range of 2-150 nm from FESEM and TEM analysis. The electrochemical studies showed that MoS_2 nanoparticles produces via such technique can be used in high-performance lithium ion batteries as they have reversible discharge capacities of in range of 800 $mAhg^{-1}$.

Wang *et al.* [15] in 2017 reported low temperature synthesis of globular MoS_2 nanoparticles with sulphur powders as sulphur source. The as-synthesized nanoparticles were characterized by X-ray diffraction (XRD), SEM, TEM for analysing structural and morphological properties. High-indexed diffraction peaks were not found in XRD patterns, which confirmed poor crystallinity and the short-range disorder exists between planes. EDX confirmed absence of impurities in the obtained sample. Raman spectroscopy was found in good agreement with XRD results. SEM and TEM reults indicated that the MoS_2 nanoparticles without $MnCl_2$ were of flower like structure with particle size 140 nm whereas NPs with traces of $MnCl_2$ have average size decreased by 50 nm. Thus, the average size of MoS_2 NPs can be reduced remarkably by introducing trace transition metals or halide ions.

Sun *et al.* [16] in 2017 synthesized MoS_2 quantum dots (QDs) cocatalysts via hydrothermal (H) and liquid exfoliation strategy (L). The as prepared QDs were homogenous with diameter of 2.49 nm and 2.27 nm, respectively. XRD, transmission electron microscopic (TEM) images and high-resolution transmission electron microscopic (HRTEM) were used to characterise the size, structure and morphology of both samples. QDs-H had very low yield and even the repeatability of experiment was poor. Moreover, they showed no better results over their bulk counterparts according to the electrochemical results. In comparison, QDs-L were observed to be highly crystalline with paralleled and ordered lattice fringes from TEM and HRTEM

images. The MoS_2 QDs-L/CdS showed higher photo and electrocatalytic hydrogen production performance.

Shomalian *et al.* [17] in 2017 synthesized porous MoS_2 nanoparticles by polymerizing complexing sol-gel method. The sample structure and size along with morphology was analysed by using data from X-ray diffraction (XRD), transmission electron microscopy (TEM), field emission scanning electron microscopy (FESEM). The nanoparticles synthesized with precursor $(NH_4)_2S_2O_8$ exhibited pure phase better than ones prepared with ammonia as precursor with continuous sulphur vapours flow. The values of band gaps were in range 2.97-2.02eV and 3.96-2.95eV with respective precursors were obtained from UV–Vis spectrophotoscopy. SEM image of the nanoparticles from ammonia has a platy and flower-like growth, whereas others have nano-plates cluster growth. The precursors and annealing temperature proved to be deciding factor of morphology of the prepared nanoparticles. TEM images of nanoparticles annealed at low temperature shows nanorods and blade like plate sections.

Sun *et al.* [18] in 2017 synthesized MoS_2/In_2S_3 ultrathin nanoflakes with mesh-shaped structure on Indium Tin Oxide (ITO) via hydrothermal method. The as-synthesized nanoflakes were characterized by X-ray diffraction (XRD), scanning electron microscopy (SEM), HRTEM, X-ray photoelectron spectroscopy (XPS), UV-visible spectroscopy and photoluminescence (PL). SEM and HRTEM analysis revealed layered nanosheets with well crystalline lattice fringes. The size of layered structure of nanosheet was found to be less than 10 nm through XRD analysis. STEM analysis showed In_2S_3 and MoS_2 were connected closely. In-doped MoS_2 was successfully observed via XPS. The as prepared composite showed higher adsorption intensity as per UV-Vis data. But, MoS_2/In_2S_3 composite showed low PL intensity, proposing to downfall in recombination. These hybrid nanoflakes have higher electrochemically active surface area (ECSA) and exhibited more superior visible light activities. They also proved to be superior photocatalyst for photoelectrochemical (PEC) cells.

Afsar *et al.* [19] in 2018 synthesized 2-D MoS_2 nanoflakes via liquid-solid phase reaction. The structure and morphology of as-obtained nanoparticles were characterized by XRD, SEM and TEM analysis. The prepared nanoflakes exhibited poly-crystalline nature. The EDS sata confirmed no impurities were present. High specific surface area of 21 m^2/g was analysed

through BET characterization. The UV-visible spectroscopy confirmed the band-gap of 2.05eV. Methylene blue (MB) and safranin-o (SO) were degraded to check the photocatalytic activity. MB was 99.58% degraded in 100 min while SO was 99.89% degraded in only 70 mins. Such obtained nanoflakes proved to be potential catalyst in waste-water treatment.

Ravikumar *et al*. [20] in 2018 synthesized 2-D nanoflowers of MoS_2 and $MoSe_2$ via simple hydrothermal method over the duration of 48 long hours. The XRD patterns referred to hexagonal phase with uniaxial tensile strain along (001) direction. HRTEM images revealed interlayer distance of 0.62 nm and showed various deformations and break-downs. The elemental distribution of Mo:S was confirmed by EDX to be 1:2. The electrochemical studies proved $MoSe_2$ to be better electrocatalyst towards HER, in reference to its higher defect level.

Song *et al.* [21] in 2018 synthesized MoS_2 nanosheets on reduced graphene oxide surface by single-step hydrothermal technique. The structural and morphological features of as-synthesized samples were characterised by XRD, FESEM and HRTEM. The patterns from XRD data referred to hexagonal phase with high degree of crystallinity. The obtained samples appeared to be highly aggregated consisting of severly stacked large-scale sheets. As observed in HRTEM, the MoS_2/RGO revealed flower-like morphology. The electrochemical experiments showed that MoS_2/RGO composite is better electrode than simple MoS_2 as it has higher cycling stability. The results concluded that introduction of graphene loosens the structure giving rise to higher acceleration of ion and electron transport, making MoS_2/RGO better electrodes for sodium ion batteries.

References

[1] K. H. Hu and X. G. Hu, "Formation, exfoliation and restacking of MoS_2 nanostructures," *Mater. Sci. Technol.*, vol. 25, no. 3, pp. 407–414, 2009.

[2] H. Lin, X. Chen, H. Li, M. Yang and Y. Qi, "Hydrothermal synthesis and characterization of MoS_2 nanorods," *Mater. Lett.*, vol. 64, no. 15, pp. 1748–1750, 2010.

[3] B. Dong, Y. M. Chai, Y. Q. Liu and C. G. Liu, "Hydrothermal Synthesis and Characterization of Novel MoS_2 Nanoflowers Directed by Lonic Liquid," *Adv. Eng. Mater. Pts 1-3*, vol. 194–196, pp. 785–789, 2011.

[4] G. Chen *et al.*, "Ball-milling combined calcination synthesis of MoS_2/CdS photocatalysts for high photocatalytic H_2 evolution activity under visible light irradiation," *Appl. Catal. A Gen.*, vol. 443–444, pp. 138–144, 2012.

[5] M. Wang, G. Li, H. Xu, Y. Qian and J. Yang, "Enhanced lithium storage performances of hierarchical hollow MoS_2 nanoparticles assembled from nanosheets," *ACS Appl. Mater. Interfaces*, vol. 5, no. 3, pp. 1003–1008, 2013.

[6] C. Zhao *et al.*, "Thin MoS_2 nanoflakes encapsulated in carbon nanofibers as high-performance anodes for lithium-ion batteries," *ACS Appl. Mater. Interfaces*, vol. 6, no. 9, pp. 6392–6398, 2014.

[7] X. Wang, Z. Zhang, Y. Chen, Y. Qu, Y. Lai and J. Li, "Morphology-controlled synthesis of MoS_2 nanostructures with different lithium storage properties," *J. Alloys Compd.*, vol. 600, pp. 84–90, 2014.

[8] S. V. P. Vattikuti, C. Byon, C. V. Reddy, J. Shim and B. Venkatesh, "Co-precipitation synthesis and characterization of faceted MoS2nanorods with controllable morphologies," *Appl. Phys. A Mater. Sci. Process.*, vol. 119, no. 3, pp. 813–823, 2015.

[9] S. V. P. Vattikuti, C. Byon and C. V. Reddy, "Synthesis of MoS_2 multi-wall nanotubes using wet chemical method with H_2O_2 as growth promoter," *Superlattices Microstruct.*, vol. 85, pp. 124–132, 2015.

[10] A. J. Cheah, W. S. Chiu, P. S. Khiew, S. Radiman and M. A. A. Hamid, "Synthesis and characterization of visible-active molybdenum disulfide (2H-MoS_2) nanospheres," vol. 020030, p. 020030, 2015.

[11] X. L. Yin *et al.*, "MoS_2/CdS Nanosheets-on-Nanorod Heterostructure for Highly Efficient Photocatalytic H_2 Generation under Visible Light Irradiation," *ACS Appl. Mater. Interfaces*, vol. 8, no. 24, pp. 15258–15266, 2016.

[12] J.-F. C. G Deokar, D Vignaud, R Arenal and P Louette, "Synthesis and characterization

of vertically standing MoS_2 nanosheets," *Sci. Rep.*, vol. 21171, no. 6, pp. 1–9, 2016.

[13] H. Yan, P. Song, S. Zhang, Z. Yang, and Q. Wang, "Facile synthesis, characterization and gas sensing performance of ZnO nanoparticles-coated MoS_2 nanosheets," *J. Alloys Compd.*, vol. 662, pp. 118–125, 2016.

[14] K. S. Kumar, W. Li, M. Choi, S. M. Kim, and J. Kim, "Synthesis and lithium storage properties of MoS_2 nanoparticles prepared using supercritical ethanol," *Chem. Eng. J.*, vol. 285, pp. 517–527, 2016.

[15] H. Wang *et al.*, "Low-Temperature Synthesis of near-monodisperse globular MoS_2 nanoparticles with sulphur powders," *Nano*, vol. 12, no. 08, p. 1750091, 2017.

[16] J. Sun, L. Duan, Q. Wu and W. Yao, "Synthesis of MoS_2 quantum dots cocatalysts and their efficient photocatalytic performance for hydrogen evolution," *Chem. Eng. J.*, vol. 332, pp. 449–455, 2018.

[17] K. Shomalian, M. M. Bagheri-Mohagheghi and M. Ardyanian, "Synthesis and characterization of porous nanoparticles of molybdenum sulfide (MoS_2) chalcogenide semiconductor prepared by polymerizing-complexing sol–gel method," *J. Mater. Sci. Mater. Electron.*, vol. 28, no. 19, pp. 14331–14340, 2017.

[18] B. Sun, F. Shan, X. Jiang, J. Ji and F. Wang, "One-pot synthesis of MoS_2/In_2S_3 ultrathin nanoflakes with mesh−shaped structure on indium tin oxide as photocathode for enhanced photo-and electrochemical hydrogen evolution reaction," *Appl. Surf. Sci.*, vol. 435, pp. 822–831, 2018.

[19] M. F. Afsar *et al.*, "Two-dimensional Molybdenum disulphide nanoflakes synthesized by liquid-solid phase reaction method: Regenerative photocatalytic performance under UV-visible light irradiation by advance oxidation process," 2007.

[20] C. H. Ravikumar, G. V. Nair, S. Muralikrishna, D. H. Nagaraju and R. G. Balakrishna, "Nanoflower like structures of $MoSe_2$ and MoS_2 as efficient catalysts for hydrogen evolution," *Mater. Lett.*, vol. 220, pp. 133–135, 2018.

[21] H. Song, A. Tang, G. Xu, L. Liu, M. Yin and Y. Pan, "One-step Convenient Hydrothermal Synthesis of MoS_2 / RGO as a High-performance Anode for Sodium-ion Batteries," vol. 13, pp. 4720–4730, 2018.

3. Experimental

3.1 Chemicals

In this study, the nanosized molybdenum disulphide has been synthesized via reduction-sulphurization method using a specially designed stainless steel autoclave. High purity precursors of molybdenum and sulphur were used for synthesis. Molybdenum trioxide (MoO_3) (*Loba Chemie*) was used as molybdenum source and sodium sulphide (Na_2S) (*Loba Chemie*) was used as sulphur source, whereas magnesium (Mg) (*SDFC Ltd.*) acted as reducing agent. The detailed route followed for synthesis is discussed in detail below:

3.2 Sample preparation

A specially designed high grade stainless steel autoclave was used for synthesis of required pure-phase molybdenum disulphide nanoparticles [1]. The precursors molybdenum trioxide (MoO_3) and sodium sulphide (Na_2S) along with reducing agent (Mg) were mixed in agate-mortar. Then, the solid mixture was transferred into the autoclave and sealed properly. The sealed autoclave was heated in furnace upto different required temperatures (300, 400, 500, 600, 700, 800 °C) for distinct holding times (8, 10, 12, 15 hours), with maintained heating rate of 5 °C/min. Optimisation in quantities of precursor's, temperature and time was done to obtain pure phase of MoS_2. The powder collected, after autoclave had cooled down to room temperature, was put into diluted hydrochloric acid for leaching. The obtained powder was washed with distilled water and dried in oven at 100 °C for duration of 24 hours. The route followed for synthesis of nano MoS_2 is schematically represented in Fig.3.1 and the variation in synthesis conditions has been listed in table 3.1.

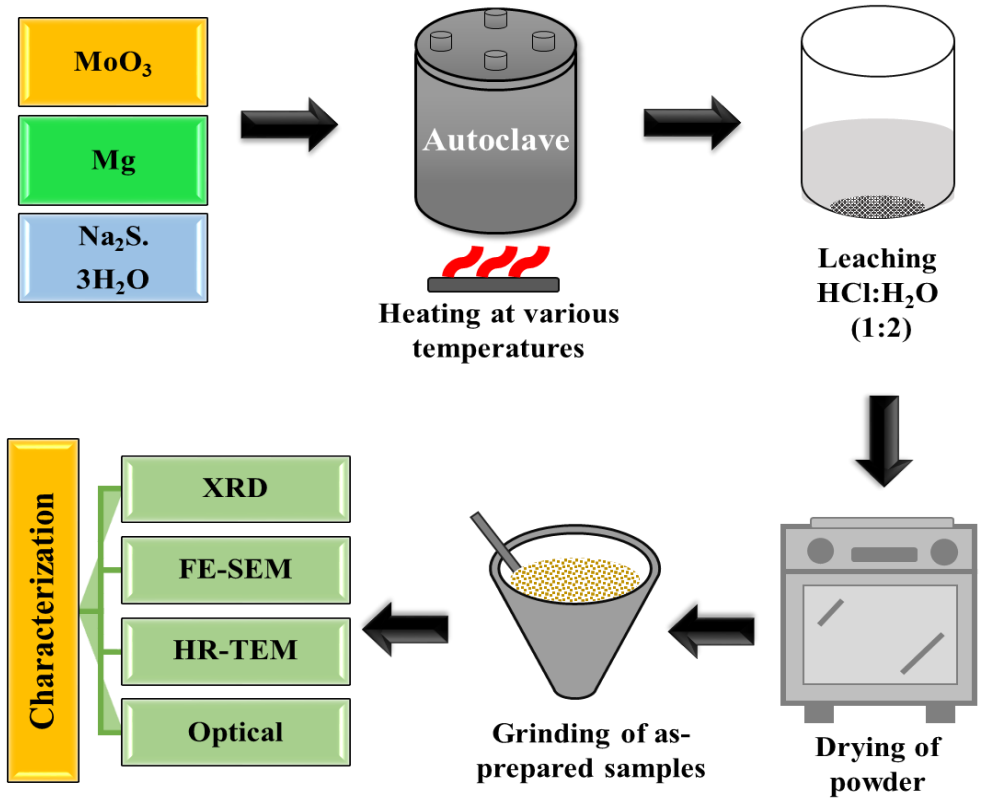

Figure 3.1: Synthesis route for preparation of MoS_2.

Table 3.1: Optimisation in synthesis conditions.

Sample Id	**MoO_3** (g)	**Mg** (g)	**$Na_2S{\cdot}xH_2O$** (g)	**Temperature** (°C)	**Holding time** (hrs)
MS-1	1.439	2.5	2	400	10
MS-2	1.439	2.5	2	500	10
MS-3	1.439	2.5	2	600	10
MS-4	1.439	2.5	2	700	10
MS-5	1.439	2.5	2	800	10
MS-6	1.439	2.5	2	500	12
MS-7	1.439	2.5	2	500	15
MS-8	1.439	2.5	3	600	10
MS-9	1.439	2.5	3	700	10
MS-10	1.439	2.5	3	700	12
MS-11	1.439	2.5	3.5	700	10
MS-12	1.439	2.5	4	700	10
MS-13	1.439	2.5	4.5	700	10

3.3 Characterization

3.3.1 X-ray diffraction (XRD)

The as-prepared samples were characterized with the help of *PANALYTICAL X'PERT PRO* XRD diffractometer armed with X'Celerator solid state detector having nickel (Ni) as an inbuilt beta filter. The Cu-Kα radiations, generated from Cu anode target material with λ=1.54443 Å, were used to detect phase and obtain crystal structure of required samples. The diffractograms with intensity versus 2θ positions, where 2θ varied in definite range of 10° to 90° with step size of 0.0170°, were recorded. The peaks as observed in this recorded XRD data were analysed by comparing them to International Centre of Diffraction Data (ICDD) cards as registered in X'pert Highscore plus software. Further, Scherrer formula was used to calculate the crystallite size.

3.3.2 Field emission scanning electron microscopy (FESEM)

In this work, morphology of the optimised samples in powder form, was determined with the help of FESEM. The images of FESEM were obtained using *HITACHI SU8010* instrument, operating at an accelerating voltage of 5 kV.

3.3.3 High resolution transmission electron microscopy (HRTEM)

The below atomic level properties of ultra-thin samples were investigated by HRTEM. A small amount of sample was placed on carbon coated grid. The as-prepared samples were characterized by *JEOL 2100* operating at a voltage of 200 kV to record TEM micrographs at various magnifications.

3.3.4 UV-Visible Spectroscopy

For the analysis of optical properties of the pure phased sample, UV-Visible spectroscopy was performed. UV-Visible reflectance spectra was carried at room temperature with *Hitachi U3900H spectrophotometer* instrument in wavelength spectral range of 200 to 800 nm. The band-gap energy of as-prepared MoS_2 was evaluated using Kubelka-Munk function, written in equation (3.1).

$$F(R) = \frac{(1-R)^2}{2R} \tag{3.1}$$

where, R stands for reflectance.

References

[1] H. Singh and O. P. Pandey, “Novel process for synthesis of nanocrystalline WC from wolframite ore,” *Ceram. Int.*, vol. 41, 2015.

4. Results and Discussion

The effects of synthesis parameters on the formation of MoS_2 nanoparticles were studied in the present work. In the primary experiments, MoO_3 (1.439g), Mg (2.5g) and Na_2S (2g) were put into autoclave at different temperatures for 10 hours. In further experiments, parameters (time, sulphur content) were varied accordingly. Finally, the obtained nanopowders were analysed by various techniques as X-ray diffraction (XRD), field emission scanning electron microscopy (FESEM), high resolution transmission electron microscopy (HRTEM) along with UV-Vis analysis for structural, morphological and optical studies, respectively.

4.1 X-ray diffraction (XRD) analysis

X'Pert HighScore Plus software was used to analyze XRD data by matching the data peaks with reference International Centre for Diffraction Data (ICDD) reference patterns. The results of XRD details revealed the presence of different phases and compounds. The list of ICDD cards, which were used in analysis, is given in Table 4.1.

Table 4.1: List of ICDD cards used for analysis of as-synthesized powders.

S.No	ICDD reference code	Compound
1	03-065-7025	MoS_2 (Hexagonal)
2	01-074-0932	MoS_2 (Rhombohedral)
3	01-089-5023	Mo (Cubic)
4	03-065-0445	Mo_2S_3 (Monoclinic)
5	01-089-5114	Mo_3S_4 (Monoclinic)
6	00-035-0609	MoO_3 (Orthorhombic)
7	01-076-1807	MoO_2 (Monoclinic)
8	01-084-1248	Mo_8O_{23} (Monoclinic)

4.1 (A) Effect of reaction temperature on synthesis of MoS_2 nanoparticles

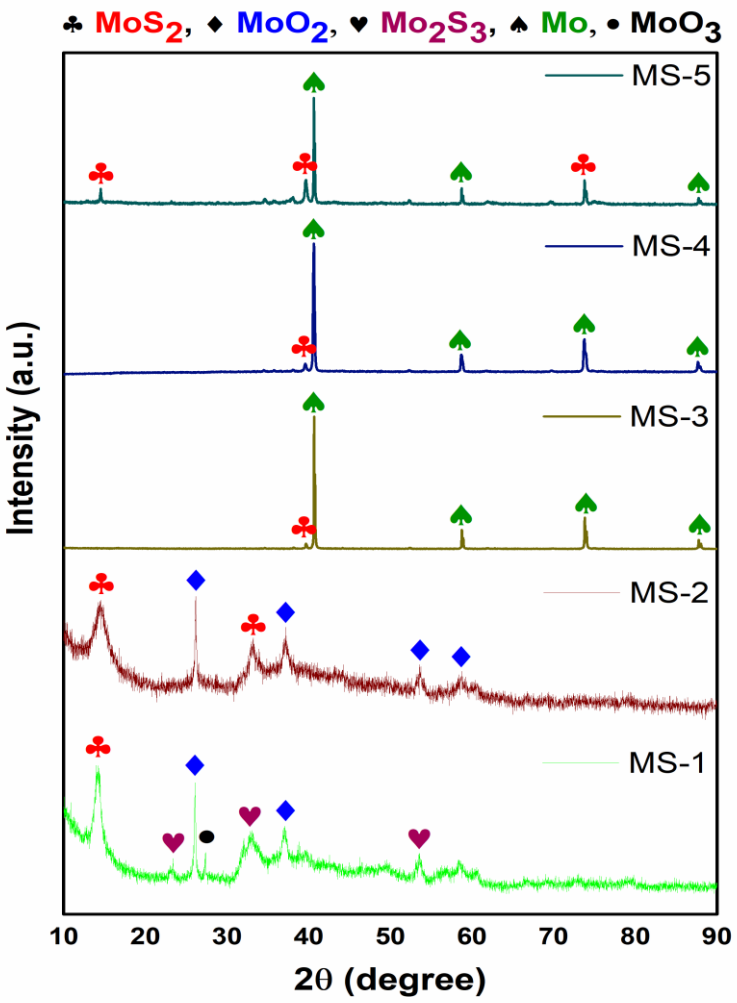

Figure 4.1: X-ray diffractograms of samples synthesized at 400 °C (MS-1), 500 °C (MS-2), 600 °C (MS-3), 700 °C (MS-4), and 800 °C (MS-5).

Figure 4.1 shows the XRD patterns of samples synthesized with variation in temperature from 400 °C to 800 °C and fixed holding time of 10 hours and heating rate of 5 °C/min. MS-1 shows formation of major peak of molybdenum disulphide (MoS_2) along with peaks of molybdenum dioxide (MoO_2) and molybdenum (III) sulphide (Mo_2S_3). The MS-2 shows formation of MoS_2 and MoO_2. No other impure phases as Mo_2S_3 were observed in MS-2. The formation of MoO_2 phase reveals that the temperature (400 °C and 500 °C) was not enough for sulphurization of reduced molybdenum dioxide phase. Therefore, the temperature was increased even further, favouring the reduction of MoO_3. At higher temperatures, (600 °C, 700°C, 800 °C) formation of molybdenum metal dominated, as only small peaks of MoS_2 were observed. The impurity

phase (Mo) present at high temperatures revealed lack of sulphur source, even if reduction process of MoO_3 to Mo metal has been accomplished. The formation of Mo metal at higher temperatures revealed the fast reduction of MoO_3/MoO_2 to Mo metal without the proper sulphurization.

4.1 (B) Effect of holding time at a particular temperature on synthesis of MoS_2 nanoparticles

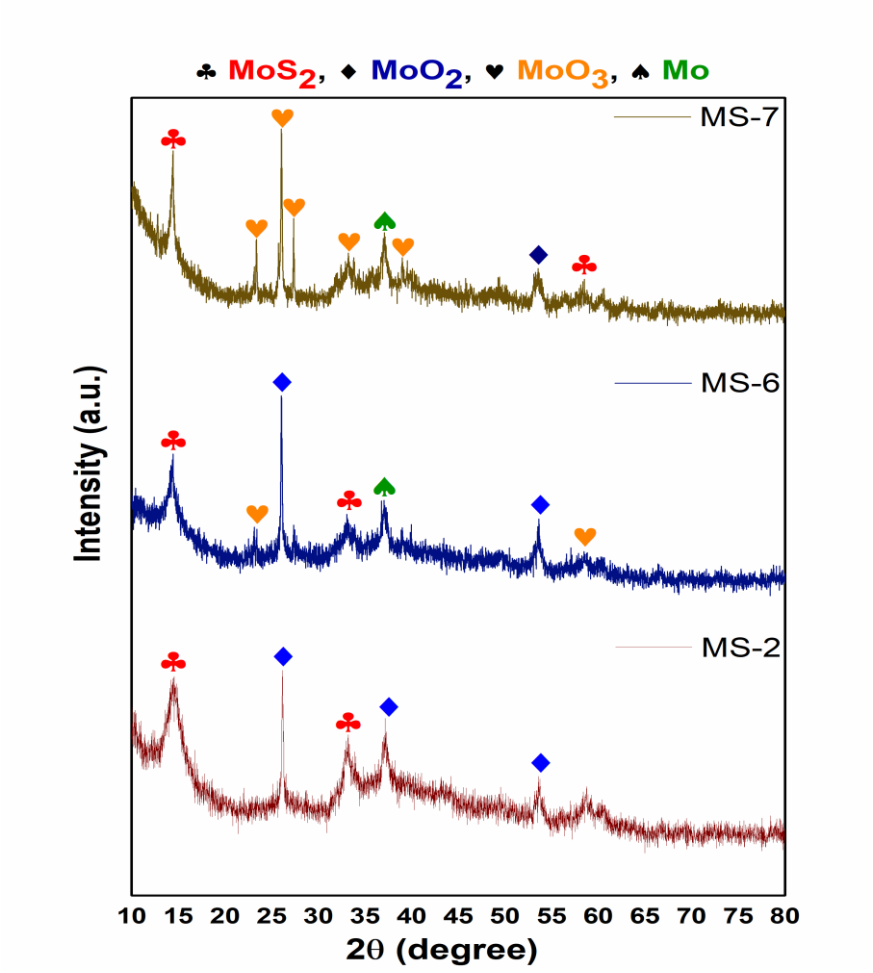

Figure 4.2: XRD patterns of samples heated for different holding times for 10 hours (MS-2), 12 hours (MS-6), 15 hours (MS-7).

Figure 4.2 reveals the X-ray diffractograms of samples synthesized at 500 °C with variation in holding times of 10, 12 and 15 hours. The major peak corresponding to MoS_2 at $2\theta = 14.398$ remained constant in all three samples, whereas the variations in impure phases was observed. When the time was increased to 12 hours (MS-6), the phase formation of Mo metal, MoO_2 and even some peaks of MoO_3 were observed, suggesting reverse oxidation of formed phase to MoO_3. Further increase in time upto 15 hours showed dominance of MoO_3 peaks indicating that MoO_2 phase has transformed into MoO_3 with increase in reaction time. The reforming of

MoO_3 could be attributed to the competition between oxygen and sulphur because of their atomic sizes. Both the oxygen and sulphur belong to the same group and oxygen being smaller gets bonded easily as compared to sulphur. The results with increase in time were not satisfactory, further more optimisation was introduced in other parameters. Afsar *et al*. [1] in 2018 synthesized MoS_2 at higher temperature (650 °C) by liquid-solid phase reaction method. Therefore, the optimisation was done at relatively higher temperatures. As observed from Fig.4.1, the reduction was complete at 600 °C and 700 °C, but sulphurization was found to be minimal; so addition in sulphur source was done in further experiments.

4.1 (C) Effect of sulphur source on synthesis of MoS_2 nanoparticles

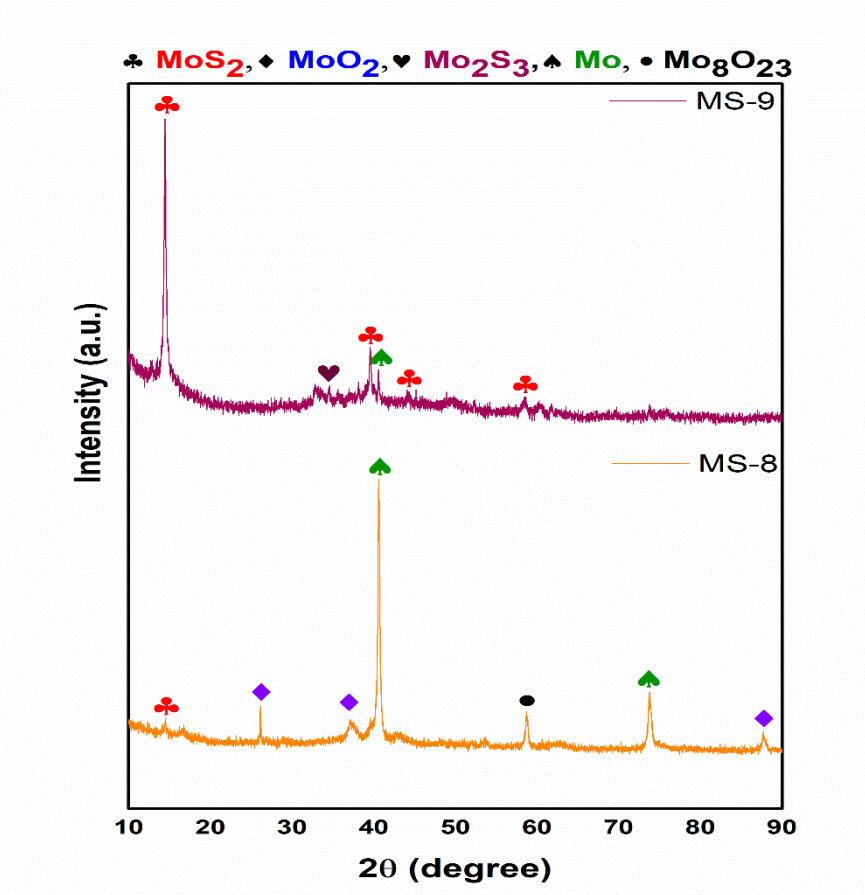

Figure 4.3: Effect of increase in sulphur source at 600 °C (MS-8) and 700 °C (MS-9).

The sulphur content was increased from 2g to 3g at 600 °C (MS-8) and 700 °C (MS-9) to enhance the sulphurization process. The XRD patterns shown in Fig.4.3 suggested that at 600 °C (MS-8) only a small peak of MoS_2 appeared along with impure phases of Mo, MoO_2 and Mo_8O_{23}. But at 700 °C (MS-9) MoS_2 phase dominated, with presence of small single peak of

Mo and Mo_2S_3 phases. The variation in sulphur content affects the formation of MoO_3 to MoS_2 as predicted in Mo and S phase diagram [2]. Therefore, the reaction temperature 700 °C revealed that the reduction and sulphurization of MoO_3 was almost accomplished. Further, to remove the impurities (Mo, Mo_2S_3) however small existing in MS-9, the holding time was increased to 12 hours (MS-10 as shown in Fig.4.4)

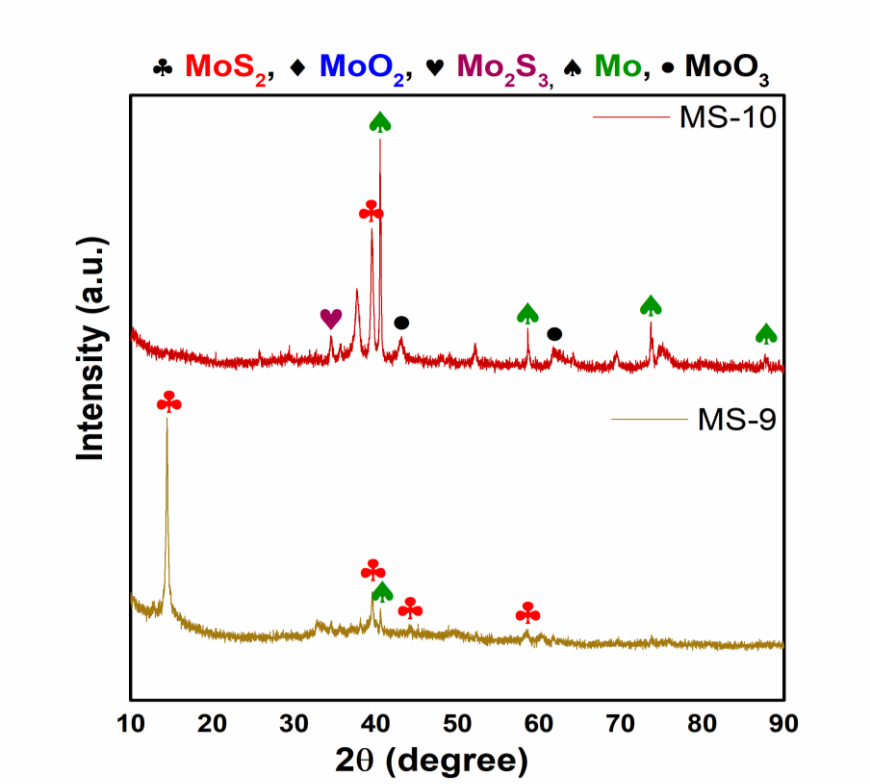

Figure 4.4: Effect of holding time for 10 hours (MS-9) and 12 hours (MS-10) at 700 °C temperature.

In the sample MS-11 (holding time of 12 hours), the impure phases as Mo_2S_3, Mo and MoO_3 along with major phase Mo were obtained. Here, also MoO_3 was obtained when holding time exceeded 10 hours. This could be the result of reverse oxidation of the formed molybdenum disulphide corresponds to the difference in atomic sizes of oxygen and sulphur. There is always a rivalry in both of them to bond with other atoms but oxygen having advantage of smaller size replaces sulphur easily at relatively higher temperatures. This could be due to presence of higher amount of oxygen as compared to sulphur inside the autoclave.

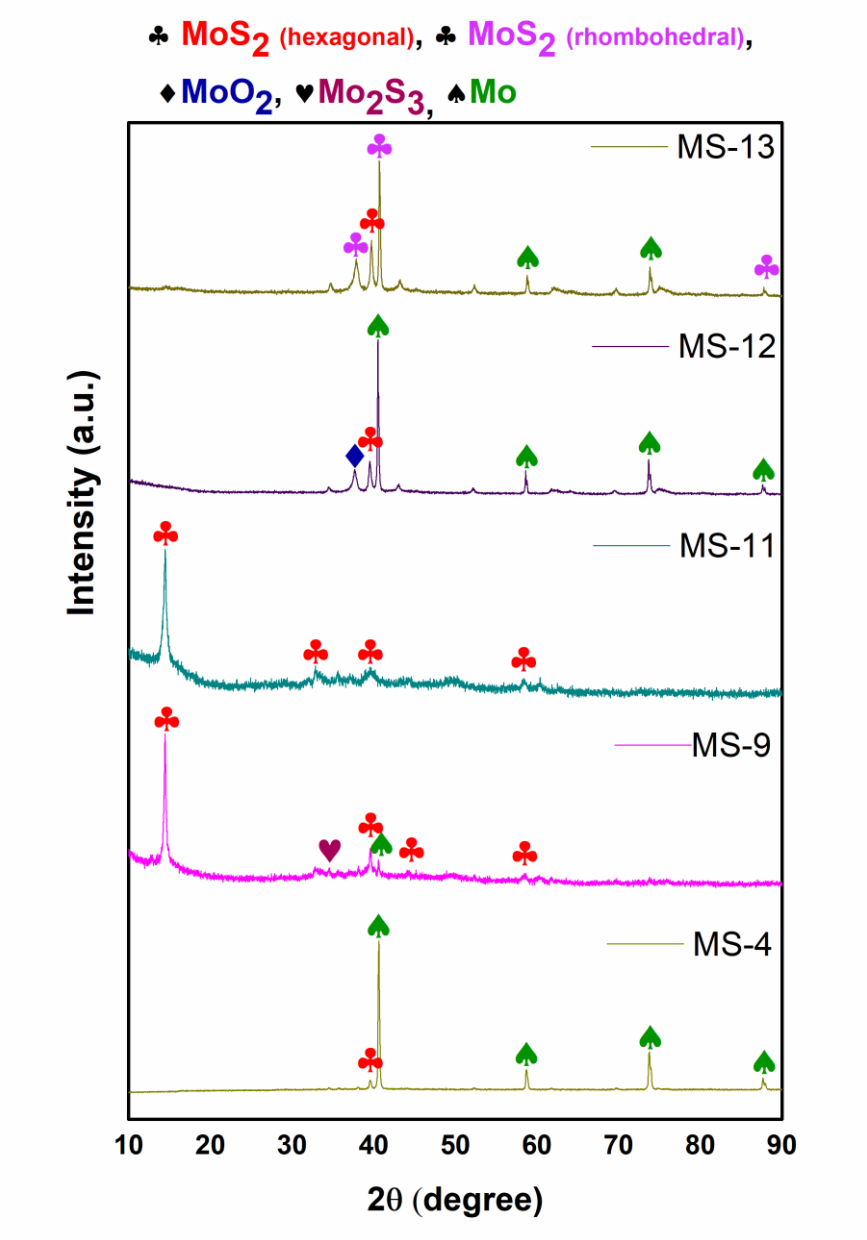

Figure 4.5: Effects of variation in sulphur source; 2g (MS-4), 3g (MS-9), 3.5g (MS-11), 4g (MS-12) and 4.5g (MS-13).

Figure 4.5 shows typical XRD patterns of samples synthesized with variation in sulphur content; 2g (MS-4), 3g (MS-9), 3.5g (MS-11), 4g (MS-12) and 4.5g (MS-13) at fixed temperature of 700 °C and holding time of 10 hours. The patterns in MS-9 (3g) showed sulphurization has been accomplished to a greater extent, but small impure intermediate phases of Mo_2S_3 and Mo metal has been detected. In an attempt to attain complete sulphurization, sulphur content was increased upto 3.5g in sample MS-11, which resulted in pure phase of MoS_2. This increase in sulphur content resulted in proceeding of reaction in forward direction.

The major peak grown at 2θ=14.398 and very small humps at higher 2θ values confirmed the synthesis of nano molybdenum disulphide. The results indicated that the as-prepared sample has amorphous nature and layers were weakly stacked [3], [4]. The further increase in sulphur content suggested in severe increase in pressure within the autoclave, as transformation in crystal structure of MoS_2 was observed. The excess amount of sulphur source used in the synthesis of sulphide compounds have considerable effects on the crystal structure [5]. The hexagonal MoS_2 has been synthesized in MS-11 (ICDD card reference code: 03-065-7025), whereas the MoS_2 synthesized with higher sulphur content (4.5g) in MS-13 exhibited rhombohedral structure (ICDD card reference code: 01-074-0932), which exists at relatively higher pressure [6], [7]. So, the results predict the effect of pressure produced inside the autoclave due to increase in sulphur content. The pressure generated inside the autoclave affects the phase formation of MoO_3 to MoS_2.

Thus, single pure phase of molybdenum disulphide was obtained at 700 °C with sulphur content of 3.5 grams (MS-11) and holding time of 10 hours. In this sample, the major peak at 2θ=14.394 corresponding to plane (002) of hexagonal MoS_2 in reference to ICDD card 03-0665-7025.

4.2 Crystallite size of single phase molybdenum disulphide

The XRD patterns are useful in determining the crystallite size and lattice parameters. Pearson VII peak function was used for curve fitting of major peak (002) in XRD pattern of pure phase MoS_2 (MS-11). The Bragg peak position and full width half maxima were marked in accordance to the best fit as shown in Fig.4.6. Scherrer formula, which is volume weighted quantity, was then taken in account for calculation of crystallite size. The Scherrer equation states the relation between Bragg peak position (2 θ) and crystallite size as:

$$D = \frac{k\lambda}{\beta cos\theta} \tag{4.1}$$

Here, D stands for calculated crystallite size, k is shape factor (0.9394), λ corresponds to wavelength of Cu Kα radiation (0.154 nm) and θ is Bragg's angle. β used in above equation refers to Bragg's peak breadth, which is amalgamation of both sample and instrumental dependent effects. The instrumental peak broadening was obtained with the help of Si standard sample and was then subtracted from observed value, so that:

$$\beta = \{(\beta^2_{observed}) - (\beta^2_{instrumental})\} \tag{4.2}$$

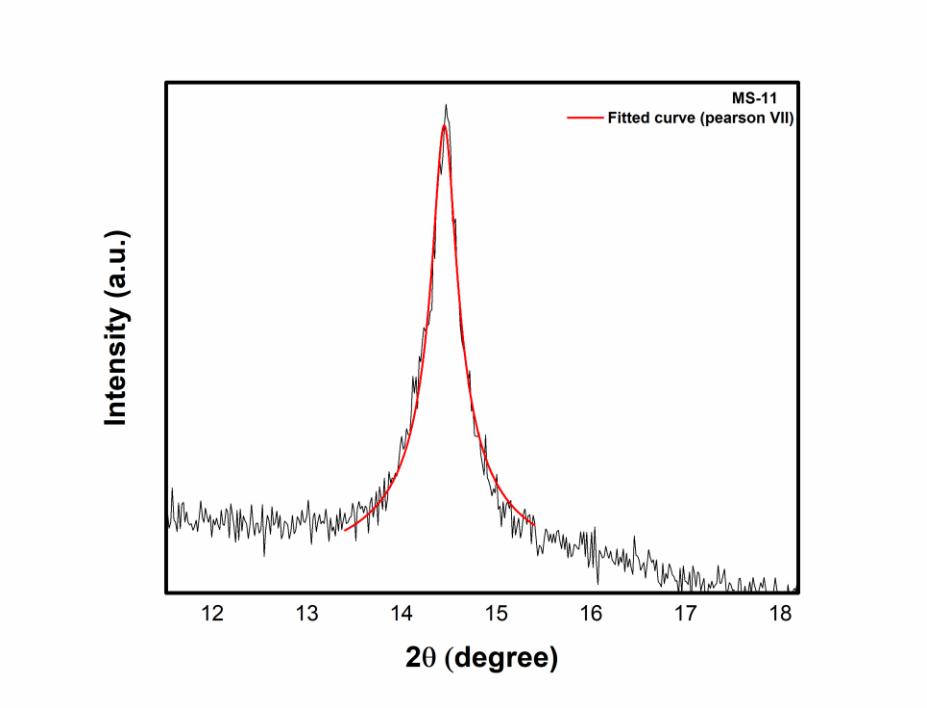

Figure 4.6: Fitting of major peak (002) using Pearson VII peak function.

Table 4.2: Crystallite size of MS-12 using Scherrer formula

Sample Id	2θ	$\beta_{observed}$	$\beta_{instrumental}$	β(radian)	cos(θ)	**D (crystallite size)**
MS-12	14.452	0.43539	0.13788	0.0072	0.99206	**19.39277 nm**

Thus, the crystallite size of single phase MoS_2 was calculated to be 19.39 nanometers.

4.2.1 Young's modulus

The synthesized pure phase MoS_2 (MS-11) exhibited hexagonal structure. To understand the elastic properties, Young's modulus ($E_{(hkl)}$) of this hexagonal structure along the best-fit plane (002) was calculated using eq.(4.3) [8].

$$E_{(hkl)} = \frac{[h^2+\frac{(h+2k)^2}{3}+\left(\frac{a}{c}l\right)^2]^2}{S_{11}(h^2+\frac{(h+2k)^2}{3})^2+S_{33}\left(\frac{a}{c}l\right)^4+(S_{44}+2S_{13})(h^2+\frac{(h+2k)^2}{3})(\left(\frac{a}{c}l\right)^2)} \quad (4.3)$$

where, S_{11}, S_{33}, S_{44} and S_{14} all are elastic compliances found by using values of elastic constants for MoS_2 hexagonal system [9]. The as calculated Young's modulus was 0.4TPa; which is in good agreement with earlier reported literature [10].

4.3 Field emission scanning electron microscopy (FESEM) analysis

The surface morphological characteristics of the sample having single phase were studied by FESEM analysis. Figure 4.7 (a) and (b) shows the micrographs of sample MS-11, synthesized at 700 °C with holding time of 10 hours. The FESEM micrographs at different magnifications shows that the particles are highly agglomerated. The results also confirm homogenous spherical/faceted morphology of particles. The size as measured from these micrographs is in range of 20-30 nm; which is approximate to the size calculated with the help of Scherrer formula in table 4.2.

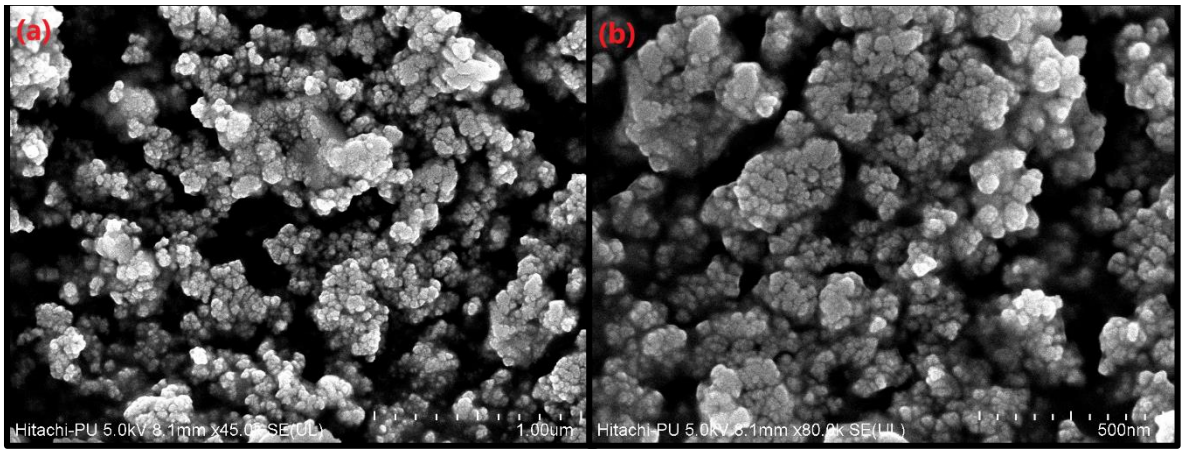

Figure 4.7: FESEM micrograph of sample MS-11 with (a) 1μm magnification (b) 500nm magnification.

4.4 High-resolution transmission electron microscopy (HRTEM) analysis

Figure 4.8 (a-d) shows the transmission electron microscopy (TEM) and HRTEM micrographs of as-synthesized nano MoS_2 particles. The TEM micrographs Fig.4.8 (a) and (b) shows the nanoflower like morphology and reveals the preferential growth of nano structures. The results are in agreement with the XRD results. Certain particles in Fig.4.8 (c) are agglomerated and possess faceted like shape which shows the resemblance to graphene and formation of nanoflakes. The HR-TEM in Fig.4.8 (d) reveals the lattice fringes of 0.327 nm corresponding to (004) plane having similar d-spacing as MoS_2 (ICDD card: 03-0665-7025). The HRTEM

confirms the pure phase formation of hexagonal MoS_2. The average particle size calculated at various areas is about ~147 nm.

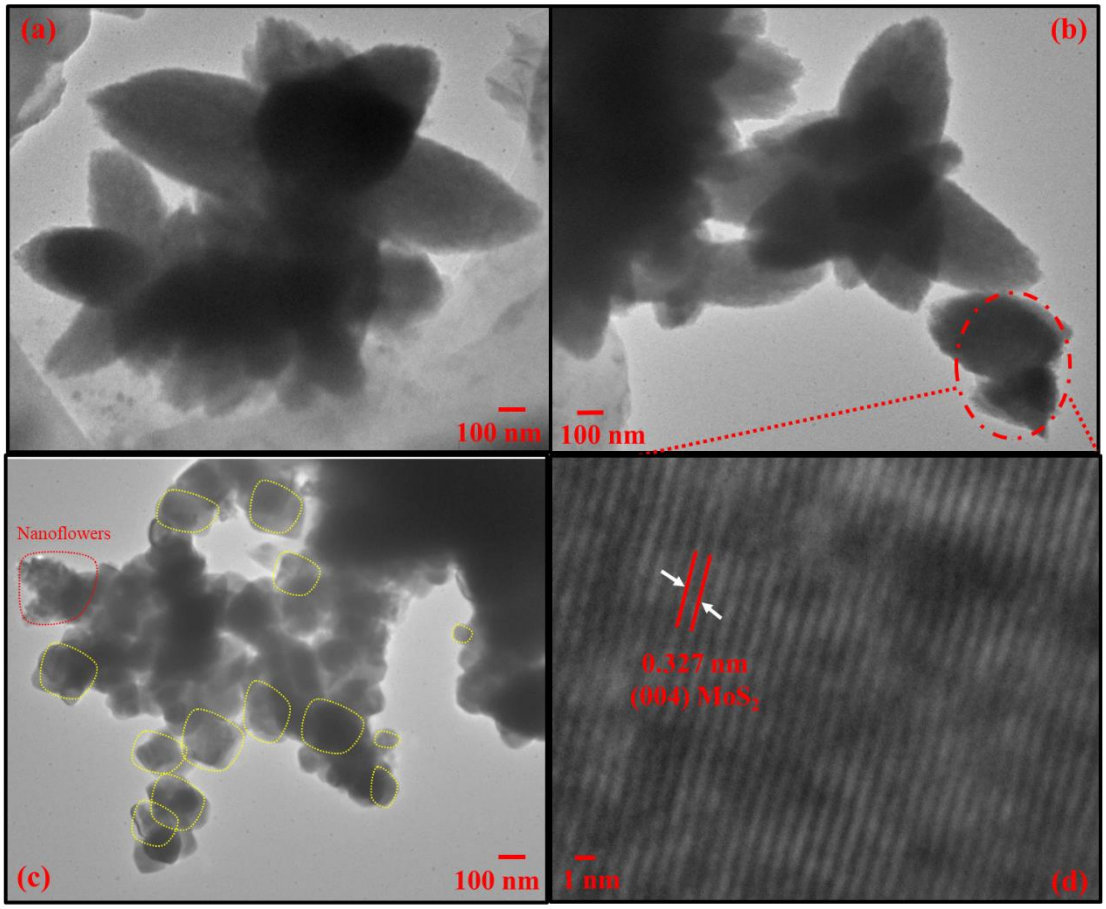

Figure 4.8: TEM micrographs of MS-11 sample; (a) and (b) shows nano-flower morphology (c) shows agglomeration of particles (d) HRTEM micrograph showing lattice fringing of sample MS-11.

4.5 UV-Visible analysis

UV-Vis reflectance spectroscopy was performed to analyze optical properties and estimate band gap energy of prepared MoS_2 sample. The Fig.4.8 shows reflectance spectra recorded in wavelength range of 200 to 800 nm at room temperature.

As the spectroscopy data was recorded for reflectance against UV-Vis rays, Kubelka-Munk function was used to find the band gap energy. According to Kubelka-Munk equation:

$$[F(R)\cdot h\nu]^n = A(h\nu - E_g) \quad (4.4)$$

where, A is proportionality constant, ν refers to frequency and E_g obtained is band gap and F(R)

is reflectance as mentioned in eq.3.1. (experimental section).

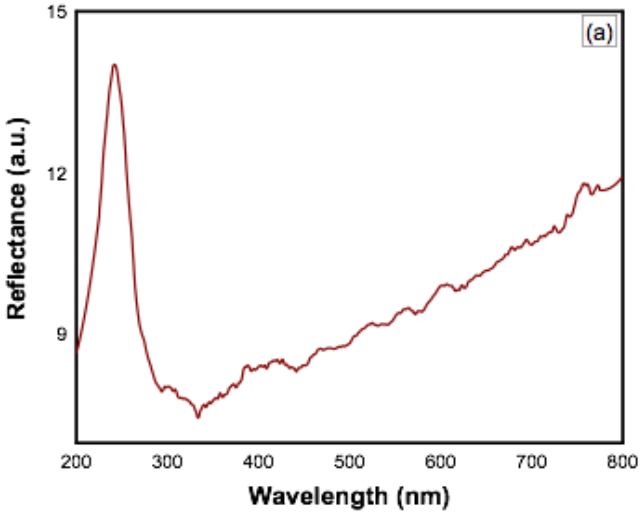

Figure 4.9: Reflectance spectra of sample MS-11.

The band gap of MoS_2 depends on its structure and morphology. Both direct and indirect band gaps for MoS_2 have been reported [11]. In the analysis of MS-11 both direct allowed (n=½) and indirect allowed (n=2) transitions are taken under consideration.

The plot between energy (hν) on X-axis vs $[F(R)\cdot h\nu]^n$ on Y-axis, where n can be ½ or 2 are plotted. The Fig.4.9 (a) shows indirect band gap with value 1.7eV and Fig.4.9 (b) shows direct band gap of 2.24eV. This blue shift in band gap energies could be attributed to the additional quantum confinement of Z-direction in as synthesized hexagonal molybdenum disulphide [12].

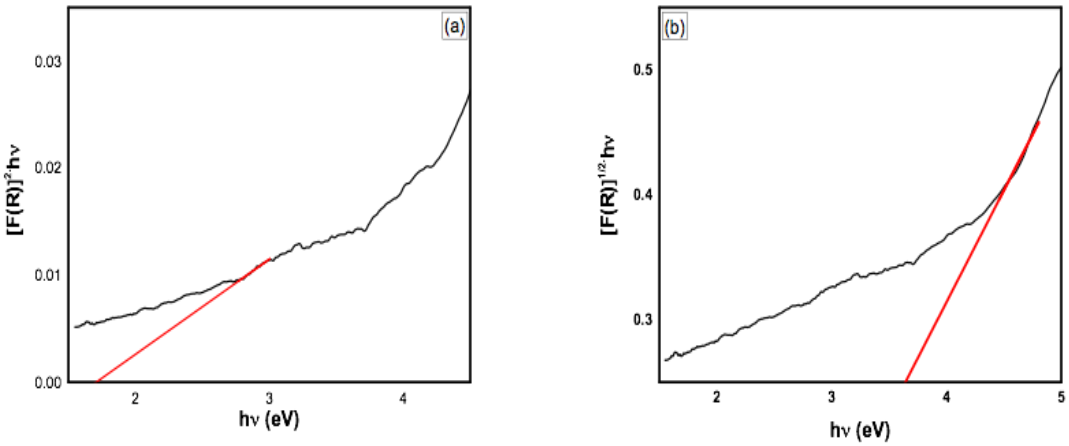

Figure 4.10: Corresponding $[F(R)\cdot h\nu]^n \sim h\nu$ curves of sample MS-11 showing (a) indirect band gap and (b) direct band gap.

4.6 Formation mechanism of molybdenum disulphide

In the present work, the nano-sized MoS_2 has been synthesized in a specially designed pressurized vessel (autoclave) via reduction-sulphurization method. The mechanism for formation of MoS_2 has been proposed on the basis of XRD results and morphological features. Mg has been added as the reducing agent, along with precursors, to favor reaction in fast forward reaction. As per reported literature, MgO catalyst is formed via interaction of Mg and oxygen present in the autoclave [13]. Then, the reduction of precursors is bought out by MgO to form H_2 and H_2S gases. Both these gases are supposed to help in reducing MoO_3 to MoO_2, owing to their diffusion coefficient [14], [15]. Smaller size of hydrogen makes it enter the grain boundaries of oxides; fragmenting them into smaller particles, whereas sulphur at same time is engaged in enclosing the particles.

As per the results revealed by XRD diffractograms for samples synthesized in temperature range 400-500 °C, the reduction of MoO_3 and simultaneous sulphurization resulted in the formation of MoO_2, MoS_2 and Mo_2S_3. The possible reaction paths taking place inside the autoclave are listed below:

$$5MoO_3 + 6Mg + 5Na_2S{\cdot}3H_2O \rightarrow MoS_2 + MoO_2 + Mo_2S_3 + MoO_3 + 10NaOH + 6MgO + H_2 + 9H_2O \quad (4.5)$$

$$5MoO_3 + 2Mg + 6Na_2S{\cdot}3H_2O \rightarrow MoS_2 + MoO_2 + Mo_2S_3 + MoO_3 + 12NaOH + 2MgO + SO_2 + 12H_2O \quad (4.6)$$

$$5MoO_3 + 5Mg + 6Na_2S{\cdot}3H_2O \rightarrow MoS_2 + MoO_2 + Mo_2S_3 + MoO_3 + 12NaOH + 5MgO + H_2S + 11H_2O \quad (4.7)$$

$$5MoO_3 + 2Mg + 7Na_2S{\cdot}3H_2O \rightarrow MoS_2 + MoO_2 + Mo_2S_3 + MoO_3 + 14NaOH + 2MgO + H_2S + SO_2 + 9H_2O \quad (4.8)$$

$$5MoO_3 + 6Mg + 6Na_2S{\cdot}3H_2O \rightarrow MoS_2 + MoO_2 + Mo_2S_3 + MoO_3 + 12NaOH + 6MgO + H_2S + H_2 + 10H_2O \quad (4.9)$$

$$5MoO_3 + 3Mg + 6Na_2S{\cdot}3H_2O \rightarrow MoS_2 + MoO_2 + Mo_2S_3 + MoO_3 + 12NaOH + 3MgO + H_2 + SO_2 + 11H_2O \quad (4.10)$$

$$5MoO_3 + 3Mg + 7Na_2S{\cdot}3H_2O \rightarrow MoS_2 + MoO_2 + Mo_2S_3 + MoO_3 + 14NaOH + 3MgO + SO_2 + H_2 + H_2S + 9H_2O \quad (4.11)$$

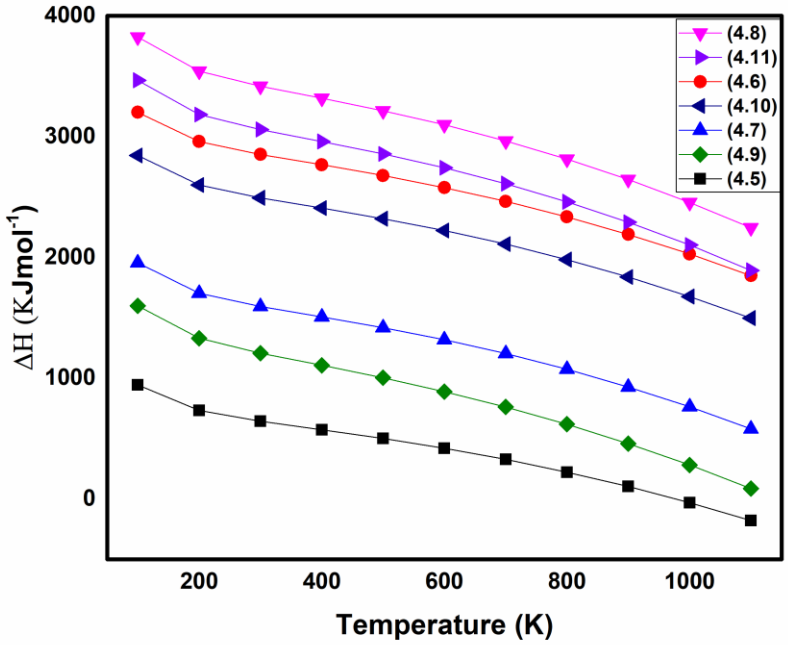

Figure 4.11: Variation in heat of formation (ΔH) corresponding to temperature (K) for reduction and sulphurization of MoO_3 into various intermediate compounds.

The graph between heat of formation (ΔH) and temperature (K) has been plotted for above reactions are shown in the Fig.4.11. The only reactions having negative values of ΔH are considered as feasible. It has been well established by the graph that only one of these reactions seems feasible only above 1000 K temperature. This indicates that along with temperature, the pressure generated in autoclave played key role in reduction of MoO_3. So, the effect of pressure along with temperature have resulted in the formation of these intermediate compounds.

However, as per reported literature, MoO_3 gets reduced to MoO_2 at the initial stages, along with evolution of some gases [15]. The possible reactions paths thermodynamically proposed are:

$$4MoO_3 + Mg + Na_2S{\cdot}3H_2O \rightarrow 4MoO_2 + 2NaOH + MgO + SO_2 + 2H_2O \quad (4.12)$$

$$MoO_3 + Mg + 2Na_2S{\cdot}3H_2O \rightarrow MoO_2 + 4NaOH + 2MgO + 2H_2S + H_2 + 2H_2O \quad (4.13)$$

$$2MoO_3 + 2Mg + Na_2S{\cdot}3H_2O \rightarrow 2MoO_2 + 2NaOH + 2MgO + H_2S + H_2O \quad (4.14)$$

$$2MoO_3 + Mg + 2Na_2S{\cdot}3H_2O \rightarrow 2MoO_2 + 4NaOH + MgO + H_2S + SO_2 + 2H_2 + H_2O \quad (4.15)$$

$$3MoO_3 + 2Mg + Na_2S{\cdot}3H_2O \rightarrow 3MoO_2 + 2NaOH + MgO + H_2 + SO_2 + H_2O \quad (4.16)$$

$$5MoO_3 + 3Mg + \frac{1}{2}Na_2S{\cdot}3H_2O \rightarrow 5MoO_2 + NaOH + 3MgO + \frac{1}{2}SO_3 + H_2O \quad (4.17)$$

$$4MoO_3 + 2Mg + Na_2S{\cdot}3H_2O \rightarrow 4MoO_2 + 2NaOH + MgO + H_2 + SO_3 + H_2O \quad (4.18)$$

Figure 4.12 depicts the relationship between heat of formation (ΔH) and temperature (in Kelvin) of the possible reactions for reduction of MoO_3 to MoO_2. It has been exhibited by the graph that reaction (4.12) is the most feasible reaction; possessing most negative value of ΔH.

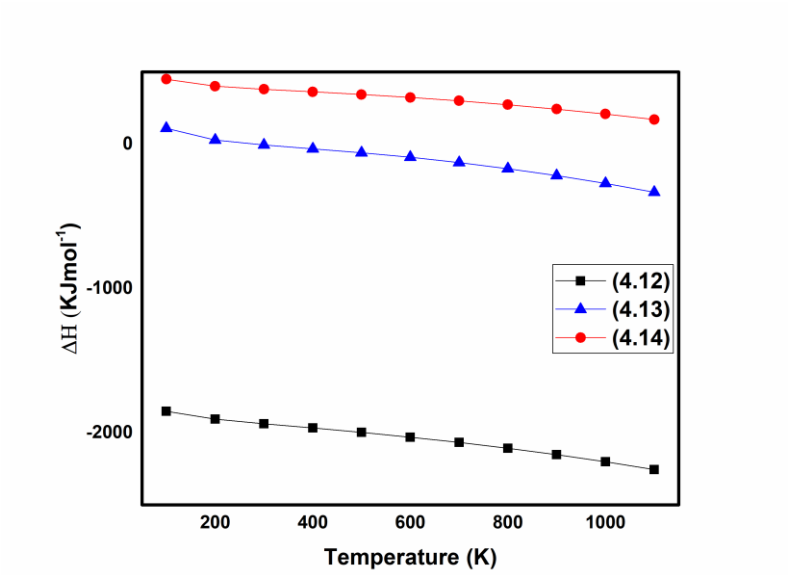

Figure 4.12: Variation in heat formation with respect to temperature (K) for reduction reaction of MoO_3 to MoO_2.

So, the reaction (4.12) is most favorable path for reduction of MoO_3 to MoO_2. However, no sulphurization has been considered till this reduction. Now, the evolved gases (H_2/H_2S) will further react to sulphurize MoO_2 to form molybdenum disulphide.

Increasing the temperature to 600-800 °C, the XRD analysis showed presence of both Mo and MoS_2 phases were present. The possible reactions based on thermodynamic kinetics for transformation of MoO_2 to MoS_2 and Mo in presence of Mg and $Na_2S{\cdot}3H_2O$ are listed below:

$$2MoO_2 + 5Mg + Na_2S{\cdot}3H_2O + H_2 + H_2S + SO_2 \rightarrow MoS_2 + Mo + 2NaOH + 5MgO + H_2S + H_2 + 2H_2O \quad (4.19)$$

$$5MoO_2 + 5Mg + 3Na_2S{\cdot}3H_2O \rightarrow MoS_2 + 4Mo + 6NaOH + 5MgO + SO_2 + 6H_2O \quad (4.20)$$

$$2MoO_2 + 4Mg + Na_2S{\cdot}3H_2O + SO_2 + H_2 + H_2S \rightarrow MoS_2 + Mo + 2NaOH + 4MgO + H_2S + 3H_2O \quad (4.21)$$

$$2MoO_2 + 6Mg + 2Na_2S{\cdot}3H_2O + SO_2 \rightarrow MoS_2 + Mo + 4NaOH + 6MgO + H_2S + H_2 + 2H_2O \quad (4.22)$$

$$2MoO_2 + 5Mg + 2Na_2S{\cdot}3H_2O + SO_2 + H_2 \rightarrow MoS_2 + Mo + 4NaOH + 5MgO + H_2S + H_2 + 3H_2O \quad (4.23)$$

$$2MoO_2 + 4Mg + 2Na_2S{\cdot}3H_2O + SO_2 + H_2 \rightarrow MoS_2 + Mo + 4NaOH + 4MgO + H_2S + 4H_2O \quad (4.24)$$

$$2MoO_2 + 3Mg + Na_2S{\cdot}3H_2O + SO_2 + H_2 + H_2S \rightarrow MoS_2 + Mo + 2NaOH + 3MgO + H_2S + H_2 + SO_2 + 2H_2O \quad (4.25)$$

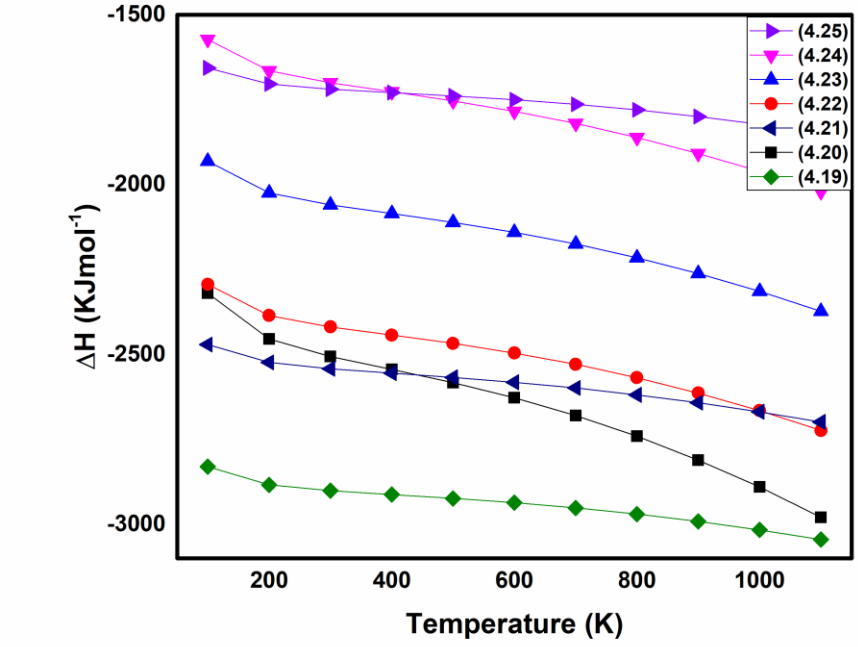

Figure 4.13: Variation in heat of formation (ΔH) with temperature (K) for further reduction of MoO_2 to form MoS_2 and Mo.

The variation in heat of formation for these above feasible reactions with respect to change in temperature, is shown in Fig.4.13. The reaction (4.19) is most feasible for synthesis of MoS_2 as it possess most negative ΔH value.

Then, for complete sulphurization sulphur content was increased. The feasible reactions at temperature 700 °C (700+343 K) for sulphurization of Mo to MoS_2 has also been listed below:

$$2Mo + 2H_2S + H_2 + Mg + 2Na_2S{\cdot}3H_2O \rightarrow 2MoS_2 + MgO + 4NaOH + 6H_2 + H_2O \quad (4.26)$$

$$Mo + SO_2 + Mg + Na_2S{\cdot}3H_2O \rightarrow MoS_2 + MgO + 2NaOH + 2H_2O \quad (4.27)$$

$$Mo + H_2S + Mg + 2Na_2S{\cdot}3H_2O \rightarrow MoS_2 + MgO + 4NaOH + 4H_2 + H_2O \quad (4.28)$$

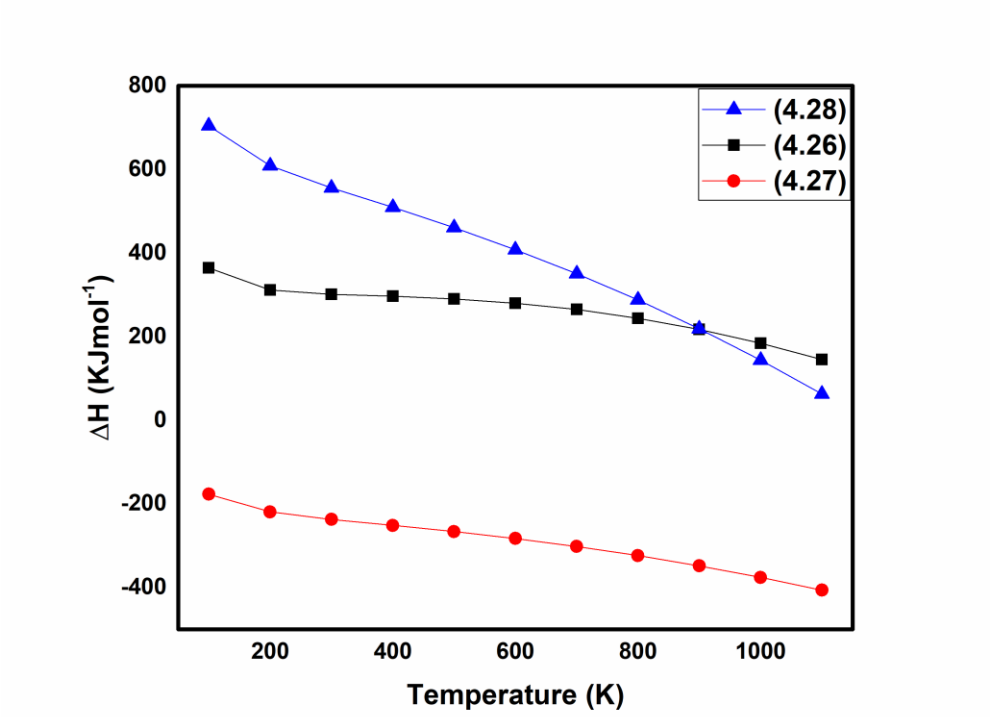

Figure 4.14: Variation of heat of formation for most feasible reaction while transformation of Mo into MoS_2.

Whereas, as per the XRD analysis, the direct formation of pure phase molybdenum disulphide is also possible inside autoclave, if adequate amount of sulphur is present. The feasibility of such transformation could occur through a number of possible reactions written below:

$$MoO_3 + Mg + 3Na_2S{\cdot}3H_2O \rightarrow MoS_2 + 6NaOH + MgO + 3H_2 + 3H_2O \quad (4.29)$$

$$2MoO_3 + Mg + \frac{9}{2}Na_2S{\cdot}3H_2O \rightarrow 2MoS_2 + 9NaOH + MgO + \frac{1}{4}H_2S + \frac{1}{4}SO_3 + \frac{35}{4}H_2O \quad (4.30)$$

$$MoO_3 + 2Mg + 3Na_2S{\cdot}3H_2O \rightarrow MoS_2 + 6NaOH + 2MgO + 2H_2S + H_2 + 4H_2O \quad (4.31)$$

$$MoO_3 + 2Mg + 2Na_2S{\cdot}3H_2O \rightarrow MoS_2 + 4NaOH + 2MgO + H_2 + 3H_2O \quad (4.32)$$

$$MoO_3 + Mg + 3Na_2S{\cdot}3H_2O \rightarrow MoS_2 + 6NaOH + MgO + H_2S + 5H_2O \quad (4.33)$$

$$2MoO_3 + \frac{1}{2}Mg + \frac{11}{2}Na_2S{\cdot}3H_2O \rightarrow 2MoS_2 + 11NaOH + \frac{1}{2}MgO + \frac{1}{2}SO_2 + H_2S + 10H_2O \quad (4.34)$$

$$MoO_3 + Mg + 2Na_2S{\cdot}3H_2O \rightarrow MoS_2 + 4NaOH + MgO + 4H_2O \quad (4.35)$$

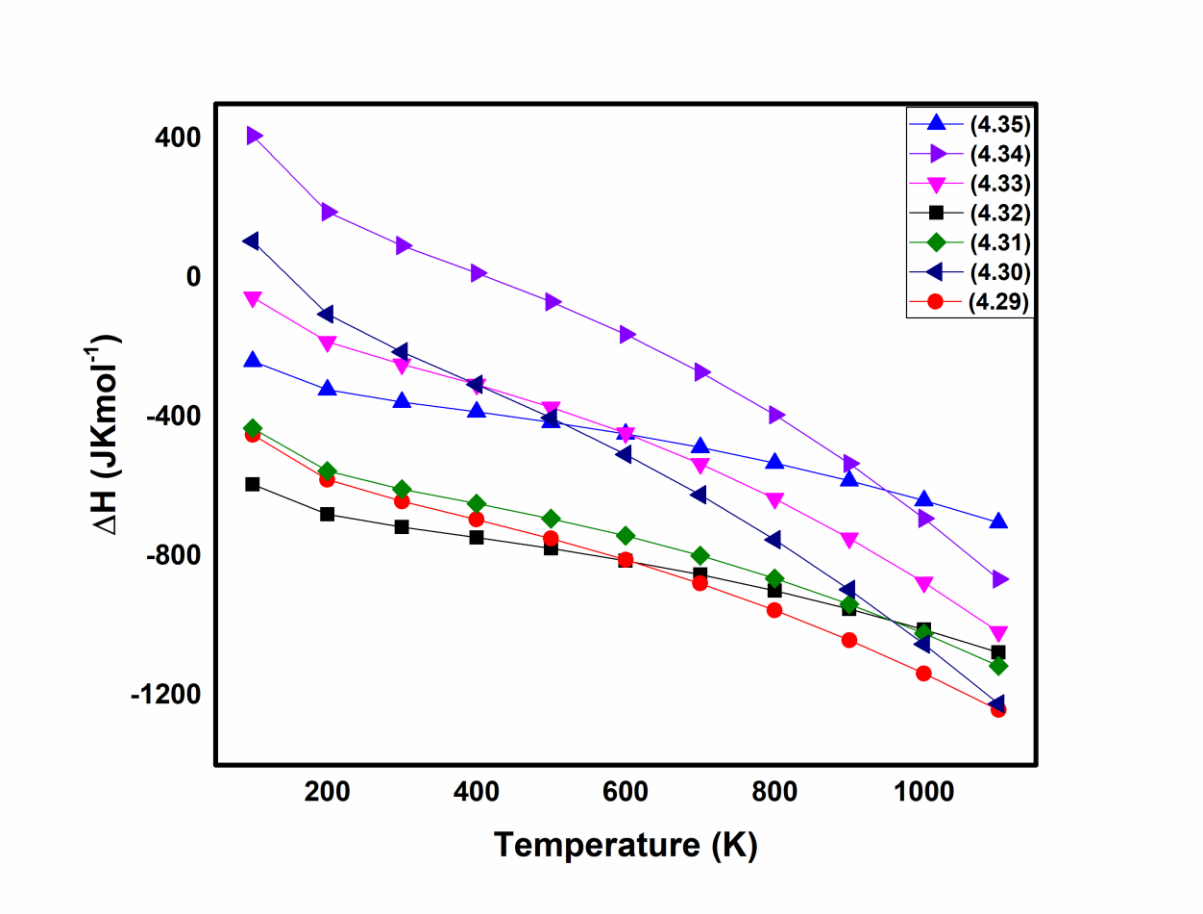

Figure 4.15: Variation in ΔH (heat of formation) with respect to temperature for direct synthesis of MoS_2 from precursors.

The reactions (4.29), (4.30) and (4.31) seems to be favorable for transformation of MoO_3 to MoS_2 in presence of Mg, $Na_2S{\cdot}3H_2O$ and pressure generated inside the autoclave. The schematic representation of synthesis mechanism as above discussed steps is shown in Fig.4.16.

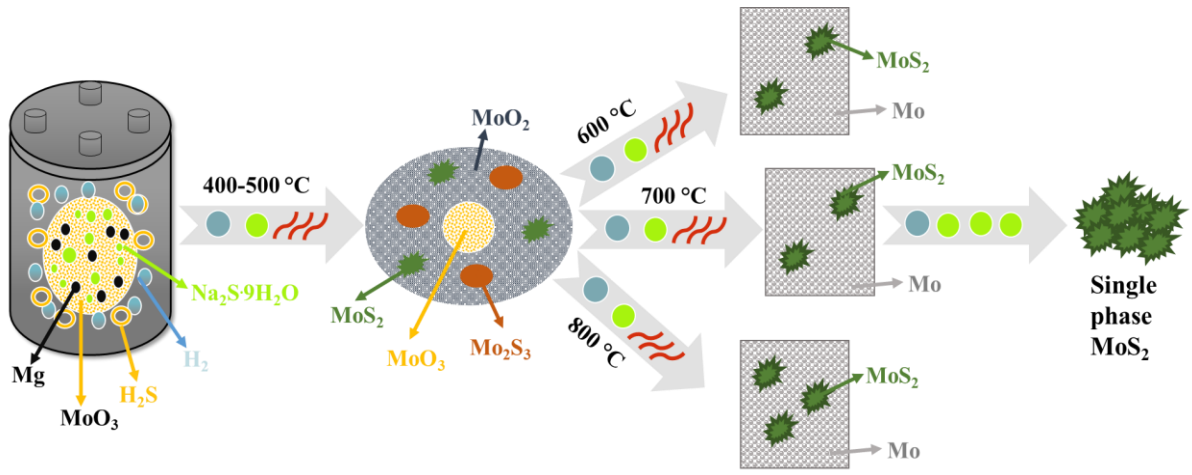

Figure 4.16: Schematic representation of synthesis of single phase nano molybdenum disulphide.

References

[1] M. F. Afsar *et al.*, "Two-dimensional Molybdenum disulphide nanoflakes synthesized by liquid-solid phase reaction method: Regenerative photocatalytic performance under UV-visible light irradiation by advance oxidation process," *Mater. Res. Express*, vol. 5, no. 5, pp. 056206, 2018.

[2] L. Brewer and R. H. Lamoreaux, "The Mo-S system (Molybdenum-Sulfur)," *Bull. Alloy Phase Diagrams*, vol. 1, no. 2, pp. 93–95, 1980.

[3] G. Li *et al.*, "Synthesis and characterization of hollow MoS_2 microspheres grown from MoO3precursors," *J. Alloys Compd.*, vol. 501, no. 2, pp. 275–281, 2010.

[4] X. L. Li and Y. D. Li, "MoS_2 Nanostructures: Synthesis and Electrochemical Mg^{2+} Intercalation," *J. Phys. Chem. B*, vol. 108, no. 37, pp. 13893–13900, 2004.

[5] B. Sheng *et al.*, "Effects of excess sulfur source on the formation and photocatalytic properties of flower-like MoS_2 spheres by hydrothermal synthesis," *Mater. Lett.*, vol. 144, pp. 153–156, 2015.

[6] Z. He and W. Que, "Molybdenum disulfide nanomaterials: Structures, properties, synthesis and recent progress on hydrogen evolution reaction," *Appl. Mater. Today*, vol. 3, pp. 23–56, 2016.

[7] A. V. Kolobov and J. Tominaga, *Two-Dimensional Transition-Metal Dichalcogenides*, vol. 239. 2016.

[8] J. M. Zhang, Y. Zhang, K. W. Xu and V. Ji, "Anisotropic elasticity in hexagonal crystals," *Thin Solid Films*, vol. 515, no. 17, pp. 7020–7024, 2007.

[9] Y. Li and R. B. Thompson, "Relations between elastic constants Cij and texture parameters for hexagonal materials," *J. Appl. Phys.*, vol. 67, no. 5, pp. 2663–2665, 1990.

[10] A. Castellanos-Gomez, M. Poot, G. A. Steele, H. S. J. Van Der Zant, N. Agra and G. Rubio-Bollinger, "Elastic properties of freely suspended MoS_2 nanosheets," *Adv. Mater.*, vol. 24, no. 6, pp. 772–775, 2012.

[11] N. Saha *et al.*, "Highly active spherical amorphous MoS_2: Facile synthesis and application in photocatalytic degradation of rose bengal dye and hydrogenation of nitroarenes," *RSC Adv.*, vol. 5, no. 108, pp. 88848–88856, 2015.

[12] G. L. Frey, S. Elani, M. Homyonfer, Y. Feldman and R. Tenne, "Optical-absorption spectra of inorganic fullerenelike MS_2 (M = Mo, W)," *Phys. Rev. B*, vol. 57, no. 11, pp. 6666–6671, 1998.

[13] R. A. Mir, P. Sharma and O. P. Pandey, "Thermal and structural studies of carbon coated Mo_2C synthesized via in-situ single step reduction-carburization," *Sci. Rep.*, vol. 7, no. 1, pp. 1–12, 2017.

[14] H. K. Sidana, R. A. Mir and O. P. Pandey, "Synthesis of molybdenum nitride (Mo2N) nanoflakes via in-situ reduction-nitridation," *J. Alloys Compd.*, vol. 736, pp. 255–265, 2018.

[15] J. Dang, G. H. Zhang, K. C. Chou, R. G. Reddy, Y. He and Y. Sun, "Kinetics and mechanism of hydrogen reduction of MoO_3 to MoO_2," *Int. J. Refract. Met. Hard Mater.*, vol. 41, pp. 216–223, 2013.

5. Conclusion

In this work, molybdenum disulphide nanoflowers were successfully synthesized via single step reduction-sulphurization method in an autoclave at 700 °C for 10 hours. The reaction parameters were optimized to obtain a pure phase MoS_2. The effect of reaction temperature, reaction time and amount of sulphur content on the phase formation were studied in detail. The estimated crystallite size of as synthesized nano crystalline hexagonal MoS_2 is 19 nm. The FESEM micrographs showed highly agglomerated particles with crystallite size in good agreement with size calculated from XRD analysis (~20-30 nm). The TEM micrographs revealed nanoflowers morphology of synthesized samples and HRTEM confirms the hexagonal phase formation of MoS_2. The optical properties studied by UV-Vis spectroscopy showing presence of both direct (2.24 eV) and indirect (1.7 eV) band gaps. The formation mechanism on the basis of XRD, morphological studies and reaction kinetics have been framed for formation of MoS_2 in a specially designed autoclave.

6. Future scope

The as-synthesized MoS_2 nanoflowers are expected to behave as promising catalysts in hydrogen evolution reaction (HER) in both photo and electro catalytic water splitting. The applications of MoS_2 as promising potential candidate for electrode material in capacitors and batteries cannot be ignored. The MoS_2 as-synthesized can be used for various sensing applications like gas sensors, optical sensors, etc. Due to its good bio compatibility, the use of MoS_2 for DNA optical detection, glucose electrochemical sensing, photo-thermal therapy and multifunctional cancer theranostic can be vastly studied. The tribiological properties of MoS_2 can also be studied for lubricant applications due to its lamellar structure and weak van der Walls forces between layers.